U.S.N.A. --- Trident Scholar project report; no. 399 (2011)

SYSTEM SIZE AND ENERGY DEPENDENCE OF STRANGENESS PRODUCTION IN 22 GEV CU+CU COLLISIONS AT RHIC

by

Midshipman 1/C Grant A. Morgan
United States Naval Academy
Annapolis, MD

Certification of Adviser Approval

Assistant Professor Richard Witt
Physics Department

Acceptance for the Trident Scholar Committee

Professor Carl E. Wick
Associate Director of Midshipman Research

USNA-1531-2

Report Documentation Page

Form Approved
OMB No. 0704-0188

Public reporting burden for the collection of information is estimated to average 1 hour per response, including the time for reviewing instructions, searching existing data sources, gathering and maintaining the data needed, and completing and reviewing the collection of information. Send comments regarding this burden estimate or any other aspect of this collection of information, including suggestions for reducing this burden, to Washington Headquarters Services, Directorate for Information Operations and Reports, 1215 Jefferson Davis Highway, Suite 1204, Arlington VA 22202-4302. Respondents should be aware that notwithstanding any other provision of law, no person shall be subject to a penalty for failing to comply with a collection of information if it does not display a currently valid OMB control number.

1. REPORT DATE	2. REPORT TYPE	3. DATES COVERED
10 MAY 2011		**00-00-2011 to 00-00-2011**

4. TITLE AND SUBTITLE	5a. CONTRACT NUMBER
System Size And Energy Dependence On Strangeness Production In 22 GEV Cu+Cu Collisions At RHIC	5b. GRANT NUMBER
	5c. PROGRAM ELEMENT NUMBER
6. AUTHOR(S)	5d. PROJECT NUMBER
	5e. TASK NUMBER
	5f. WORK UNIT NUMBER
7. PERFORMING ORGANIZATION NAME(S) AND ADDRESS(ES) **U.S. Naval Academy,Annapolis,MD,21402**	8. PERFORMING ORGANIZATION REPORT NUMBER
9. SPONSORING/MONITORING AGENCY NAME(S) AND ADDRESS(ES)	10. SPONSOR/MONITOR'S ACRONYM(S)
	11. SPONSOR/MONITOR'S REPORT NUMBER(S)

12. DISTRIBUTION/AVAILABILITY STATEMENT
Approved for public release; distribution unlimited

13. SUPPLEMENTARY NOTES
TRIDENT Reports

14. ABSTRACT

15. SUBJECT TERMS

16. SECURITY CLASSIFICATION OF:			17. LIMITATION OF ABSTRACT	18. NUMBER OF PAGES	19a. NAME OF RESPONSIBLE PERSON
a. REPORT **unclassified**	b. ABSTRACT **unclassified**	c. THIS PAGE **unclassified**	**Same as Report (SAR)**	**70**	

Abstract

The Relativistic Heavy Ion Collider (RHIC) at Brookhaven National Laboratory collides different ions at a wide variety of energies in order to study the properties of nuclear matter in extreme conditions. Beams of ions are sent around an accelerator ring at relativistic speeds approaching the speed of light before they meet in an extremely high temperature collision. The Solenoidal Tracker at RHIC (STAR) experiment exists to examine and identify the particles produced in these collisions in order to gather information about the behavior of quarks and gluons, the smallest known building blocks of matter. The strange quark is of particular interest since no strange quarks are sent into the collision. Consequently, the existence of particles with strange quarks, such as K0-shorts, Lambdas, and Anti-Lambda baryons, shows that strange quarks were produced from the energy of the collision. Particles carrying strange quarks ("strangeness"), therefore, carry information about the matter produced in the collision. This matter is believed to be quark-gluon plasma, a state in which quarks and gluons become deconfined in a space of extremely high energy and temperature.

This project determines the yield of strange quarks through measurements of K0-short mesons as well as Lambda and Anti-Lambda baryons in collisions of copper nuclei conducted at 22 GeV, one of RHIC's lowest collision energies. The measurement of strangeness production for varying ranges of beam energy contributes to the overall understanding of the phase diagram for nuclear matter. The relatively low collision energy aids in the search for a critical point in

nuclear matter phase transition. This project compares strangeness yields and spectra with current results from collisions at other beam energies and system sizes to allow better understanding of the properties of nuclear matter in extreme conditions.

Keywords: STAR, RHIC, quark-gluon plasma, strangeness, heavy ion, particle accelerator

Acknowledgments

First, I must thank Professor Richard Witt for his countless hours of instruction, explanation, and encouragement. This project would not have been remotely possible without his patience with me and passion for the subject. I would also like to thank the STAR Collaboration for their help during the entire process and for allowing me to work with the dataset of copper nuclei collisions at 22 GeV per nucleon collected at RHIC in 2005. I also must thank Professor Wick and the Trident Committee for their support and guidance at all points during the project. Finally, I would like to thank my parents for their efforts homeschooling me for 12 years, equipping me with the academic skills I needed to complete this project.

"In the beginning you laid the foundations of the earth,
and the heavens are the work of your hands." Psalm 102:25 *[NIV]*

Table of Contents

List of Figures

Chapter 1 - Introduction

In the search for knowledge, scientists have explored the world on both large and small scales. Often, scientific investigations involve entities that surround the scientists searching for them, but are difficult to observe because of the extremely large or small scales involved. The search for the minute details of the universe's construction inevitably leads to the field of particle physics. This field examines the properties of the smallest building blocks that make up the universe. This project will examine the properties of these tiny quarks, as they are called, and gluons, the particles that bind quarks, using data collected from RHIC, the Relativistic Heavy Ion Collider as the way to indirectly observe these small entities.

This chapter will begin with a discussion of nuclear matter in order to give the reader a baseline for understanding quarks, gluons, and the interactions between them. It will proceed to explain a state of nuclear matter known as quark-gluon plasma and give a description of the motivation for this field of physics, specifically as it pertains to this experiment. Finally, it will provide a brief outline of the material contained in this paper.

1.1 Nuclear Matter

The smallest known building blocks of nuclear matter are known as quarks [1]. Currently, physicists are aware of six types of quarks, which have been arbitrarily named: up, down, strange, charm, bottom, and top. Each quark also has a corresponding anti-quark, which

is simply an anti-matter quark that is identical to its matter counter-part, but having the opposite electrical charge. These quarks are never observed alone, but are observable in the form of baryons (3 quarks) or mesons (a quark-anti-quark pair). The observable world is composed of protons and neutrons, which are examples of baryons, and electrons, which are examples of leptons. Strange baryons, which are the focus of this research project, are composed of one strange quark, one up quark, and one down quark. While there are many different properties governing how different quarks will combine to form baryons, there are three specific baryons that are important to this project: the Lambda (Λ), the Anti-Lambda (Anti-Λ), and the K0-short (K_S^0) [2]. These baryons each contain at least one strange or anti-strange quark. Quarks are are bound together by the exchange of gluons, which act as the mediating particle for the strong nuclear force, much like the graviton is theorized to transmit the gravitational force [3]. Figure 1 provides a visual example of the way quarks are bound together by the exchange of gluons.

1.2 Quark-Gluon Plasma

Collisions in nuclear accelerators, such as RHIC, are theorized to create an extremely hot plasma composed not of atoms, protons, or neutrons, but of quarks and gluons. This dense stew of quarks and gluons is called "quark-gluon plasma" (QGP) [1]. Physicists are examining the baryons formed and the particles that escape collisions in order to investigate the properties of QGP.

When nuclei collide at high energies, some quarks and gluons stream away from the collision and fragment, forming jets. Since momentum must be conserved, a jet exiting one side of the collision should have a corresponding jet moving away from the collision on the other side. This is not observed in central heavy-ion collisions at RHIC. Instead, a jet may appear on

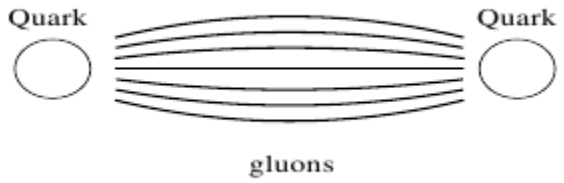

Figure 1: Quarks and Gluons [2]

one side of the collision area with no corresponding jet on the other side to conserve momentum [2]. These suppressed jets, as they are called, suggest that the quarks and gluons from which the baryons and hadrons are formed interacted with and lost energy in some sort of liquid or plasma before exiting the collision area [1]. This substance is theorized to be quark-gluon plasma.

During the collisions at RHIC, the QGP phase occurs immediately after the collision. After the QGP expands and begins to cool, the temperature and density of the quarks and gluons becomes too small to maintain QGP. At this stage, a hadronic gas is formed as the quarks and gluons form hadrons in a process called hadronization and leave the collision area [2]. The temperature at which this occurs is called the "freeze-out" temperature.

Nuclear matter can potentially exist in three states: hadronic matter, deconfined matter, and a mixed phase [2]. Heavy ion physicists are searching for the critical point in the nuclear matter phase diagram where a cross-over transition of nuclear matter becomes a first-order transition between hadronic matter and QGP. Thus far, it has been difficult for physicists to determine the exact location of the critical point. Figure 2 is a diagram that shows the critical point as a cross between the first-order and cross-over transition between hadronic matter and QGP. The character of this transition may vary depending on the temperature of the collision and the size of the colliding particles. For this reason, it is helpful to analyze systems with different sized nuclei entering the collision and at different energy levels since the transition may have a dependence on baryon density and collision energy.

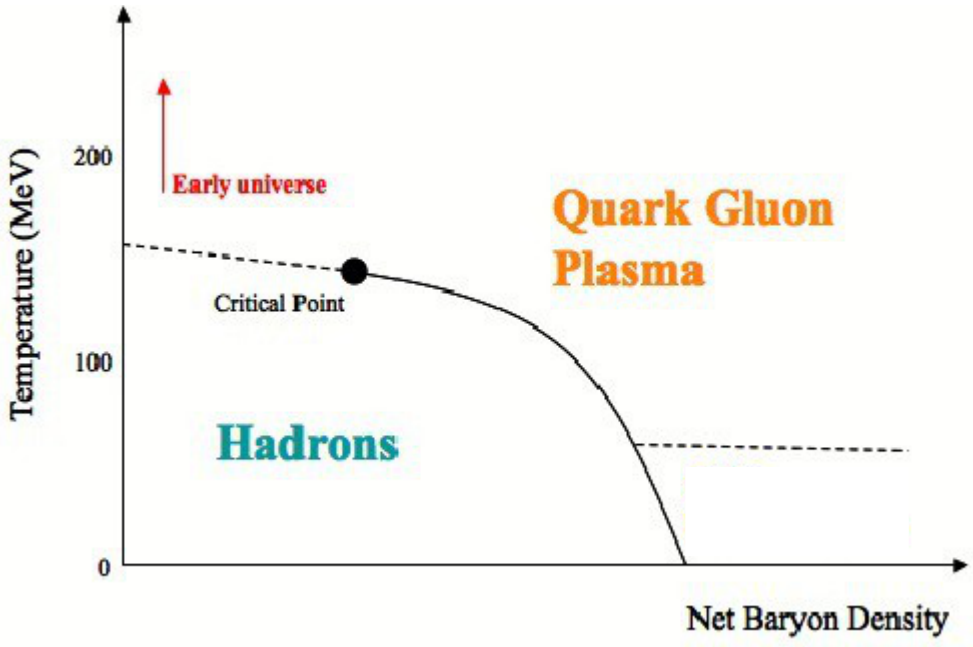

Figure 2: Quark-Gluon Plasma and the Critical Point [3]

1.3 Motivation

Strangeness is of particular importance to this project because baryons containing strange quarks are produced in high energy relativistic reactions even through strange quarks are not present in the incident nuclei. As a result, any particles that exit the collision with a strange quark signify that the matter entering the collision must have been converted to some form of energy before re-emerging as matter again. This is an application of Einstein's famous equation $E=mc^2$, which shows mass and energy to be different manifestations of matter. In other words, mass and energy are equivalent according to a factor of the speed of light squared. In our experiment, matter becomes part of a region of high energy density (QGP) and leaves again in the form of particles [2]. A baryon with a strange quark, therefore, has a particle that resulted from the energy present in the QGP; therefore, strangeness is a way of quantifying the

deconfinement of quarks and gluons.

Also of importance is finding anti-quarks, that is, quarks that form anti-baryons or anti-matter. Since no anti-matter was inserted into the collision, scientists know that any anti-particle resulting from a collision must have been formed in the energy present. Anti-Λ particles are an example of baryons composed of anti-matter. In an ideal experiment, all baryons would completely participate in a collision, and there would be no lingering or fragmented baryons left in the collision area. In this case, a quantity called the "baryon number" would be zero. Whenever an anti-baryon is formed from the energy of the collision, its counter-part composed of matter must also be formed. This means that for every Anti-Λ created from the collision energy, there must also be a Λ formed. In the ideal case described above, the number of Anti-Λ's would equal the number of Λ's that exit the collision region. In an actual experiment, however, the region is polluted by baryons, and the baryon number is greater than one. Since the baryon number must be conserved, there must be an excess of baryons that are found in the experiment when compared to anti-baryons. Thus, the ratio of Anti-Λ to Λ particles that exit the collision area will reveal the degree to which the area is "baryon free." In other words, it will reveal the degree to which the incoming baryons in the colliding nuclei influence the particle production.

Quark-gluon plasma is of interest to particle physicists for many reasons. On a fundamental level, intellectual curiosity drives the search for QGP, its critical point, and its properties. It is also hypothesized that QGP played a role in the first moments of the universe [1]. Such a scientific investigation may also open up the doors to more discoveries in the realm of particle physics in the future. In a young scientific field such as heavy ion physics, answers lead to even more questions, questions that this project will help answer.

1.4 Overview

This paper will begin by describing RHIC and the Solenoidal Tracker at RHIC (STAR). After explaining some of the details about how the experiment and detector work in Chapter Two, Chapter Three will describe the analysis of the dataset collected by STAR, which recorded the results of copper ions colliding at an energy of 22 GeV (giga electron-volts) per nucleon. After showing the statistical analysis and cuts applied to the data in Chapter Three, the paper will explain the acceptance and efficiency corrections process and show the finalized results in Chapter Four. Finally, Chapter Five will discuss the physics implications of the results, specifically focusing on the role that the energy of a collision and the size of the ions have in particle production in general and strangeness production in particular. The results in this experiment will be compared to the results of other experiments at different energies with different system sizes. Chapter Six will give a brief conclusion for the project.

Chapter 2 – STAR Experiment

While the most famous particle accelerator is the Large Hadron Collider (LHC) at CERN in Switzerland, RHIC was the first heavy-ion collider, predating LHC by more than ten years. This chapter will explain the process by which RHIC accelerates ions to relativistic speeds. It will then discuss how the STAR experiment within RHIC is able to detect collisions and reconstruct particle tracks from the data it collects.

2.1 Relativistic Heavy Ion Collider (RHIC)

The Relativistic Heavy Ion Collider (RHIC) is located at Brookhaven National Laboratory on Long Island. It was designed to collide two beams of nuclei at relativistic speeds very near the speed of light. The accelerator at RHIC is a combination of many different elements. A beam of heavy ions, nuclei stripped of their electrons, are accelerated through a tandem accelerator until the beams reach an energy of approximately 30 MeV (mega electron-volts) per nucleon [4]. The beam then enters the Alternating Gradient Synchrotron (AGS), which continues to accelerate the beams to an energy on the order of 10 GeV per nucleon [4]. Finally, the beam is split into two beams and enters the main circular track of RHIC. The beams are then accelerated in opposite directions around two 3.8 kilometer rings.

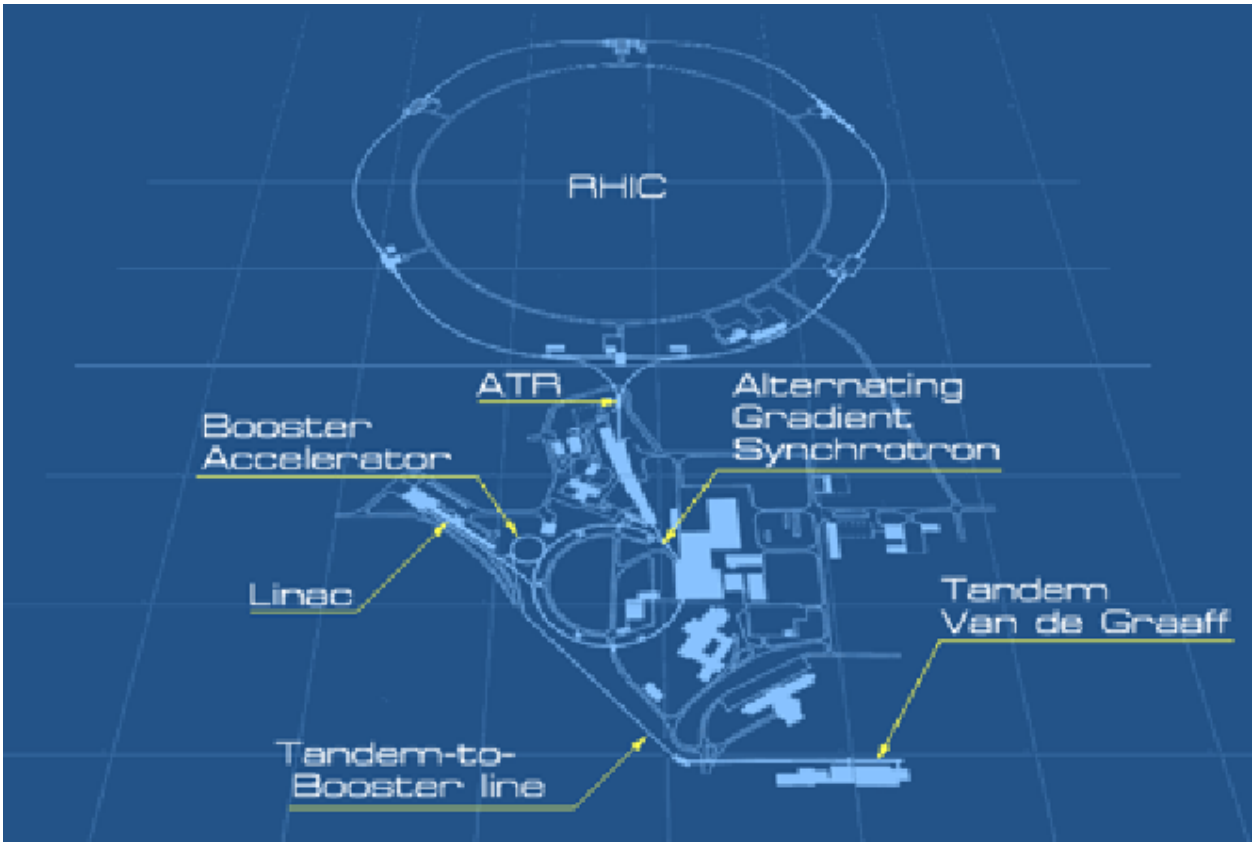

Figure 3: RHIC Accelerators [7]

Figure 3 shows the path of an ion beam through the different components of RHIC. Hundreds of superconducting magnets, cooled by helium, direct the beams around the underground circular track [1]. Figure 4 shows the author standing next to the underground rings at RHIC. At six different locations the two rings cross, allowing the beams to collide. Four of the collision sites have their own detector, which are designed to look at specific aspects of these collisions. The four detectors are BRAHMS, PHENIX, PHOBOS, and STAR.

Figure 4: The author and MIDN Campos standing next to the accelerator ring at RHIC.

2.2 Solenoidal Tracker at RHIC (STAR)

The Solenoidal Tracker at RHIC (STAR) is a three-story high cylinder equipped with magnets, detectors, and other electronics to act as a huge "digital camera" for examining the collisions at RHIC [1]. It detects the particles that emanate from the collisions produced by RHIC. Figure 5 shows an image of particle tracks collected in one of the first collisions to take place at the STAR

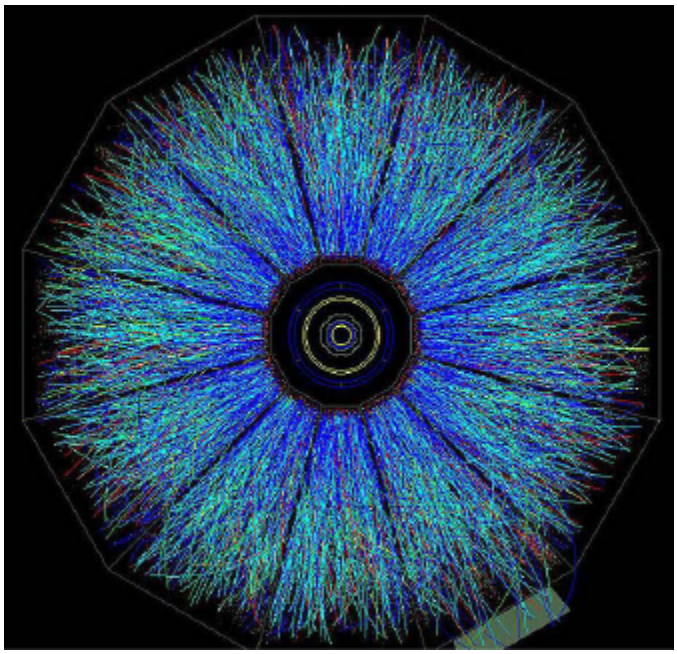

Figure 5: First Collisions at RHIC [STAR Collaboration]

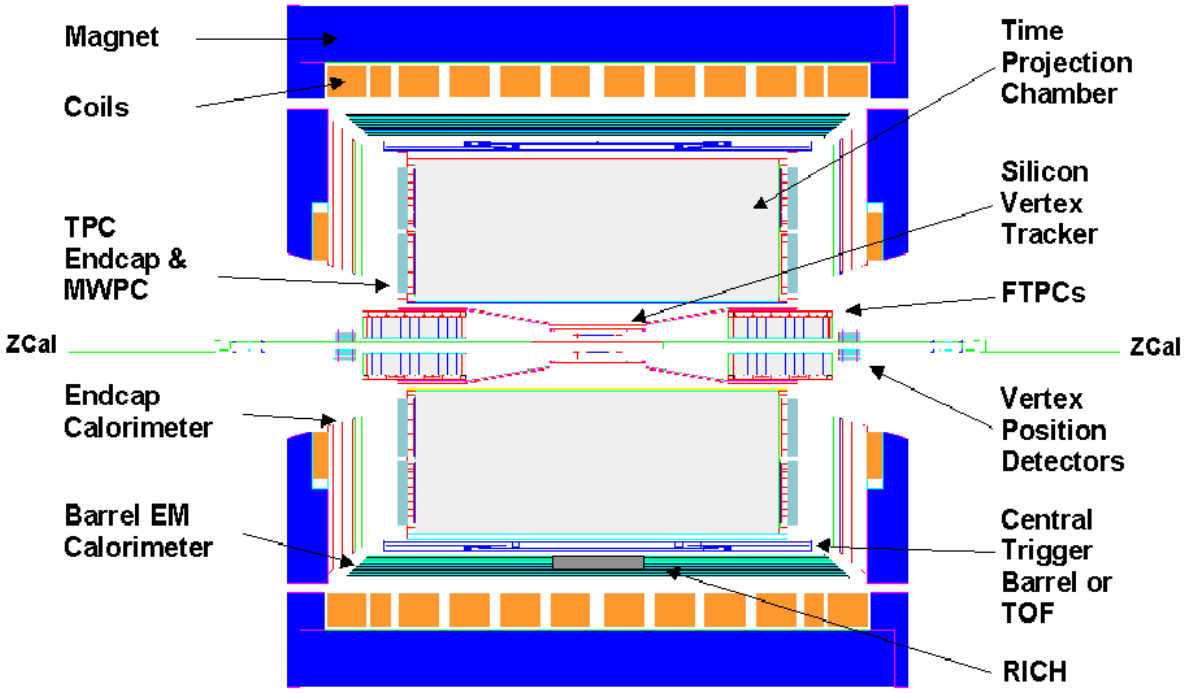

Figure 6: The STAR Detector [5]

Detector. STAR has collected a great amount of data, more than one billion events overall, from the many runs it has conducted over the past ten years, including collisions at both high and low energies and with different sized ions. STAR currently collects more data than can even be analyzed by physicists today. The data being analyzed in this experiment has been waiting for analysis since its collection in 2005. Figure 6 provides a view of the STAR detector. STAR contains many detector subsystems inside of a 0.5 Tesla solenoid, with the primary detector being the Time Projection Chamber (TPC) [5]. Figure 7 shows STAR and the TPC. The beam pipe is shown entering the detector from the right side of the picture. As it enters, it is surrounded by a large solenoidal magnet and the TPC.

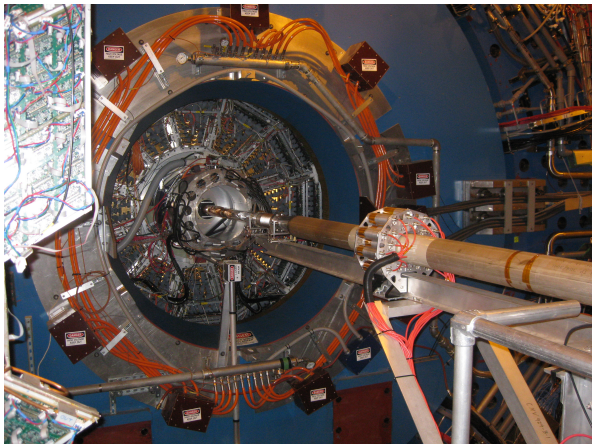

Figure 7: STAR and the TPC

2.2.1. Time Projection Chamber

The Time Projection Chamber (TPC) is a cylinder filled with gas; it is 4.2 meters long, has a diameter of 4 meters, and is shown in Figure 8 [5]. It is the heart of the STAR detector. A magnetic field created by the solenoidal magnet surrounding the TPC is parallel to the electric field created by the central cathode plane, which is maintained at a voltage of about 31 kilovolts [5]. The magnetic field created gives charged particles helical trajectories as they pass through the chamber. By taking the radius of curvature R of the particles, their charge q, and the magnetic field strength B, the transverse momentum of the particles p can be calculated by the equation p_t=0.3qBR [2].

The charged particles passing through the TPC ionize the gas inside and liberate

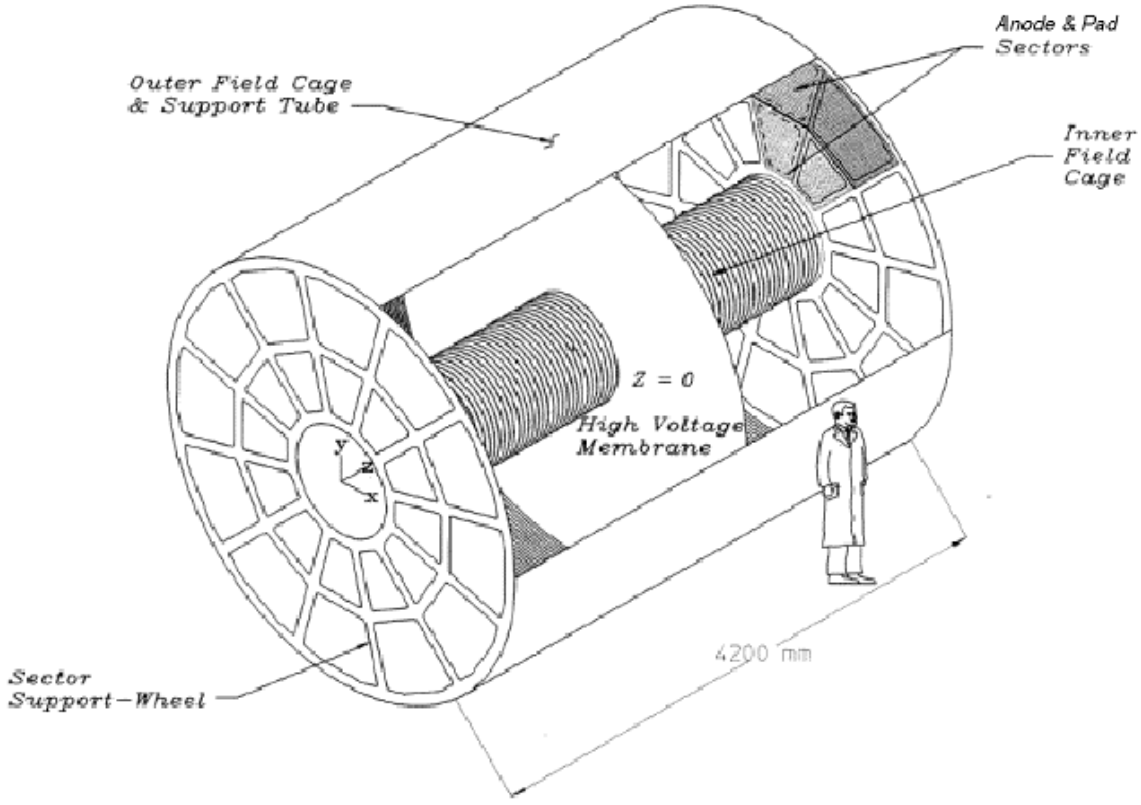

Figure 8: The Time Projection Chamber [6]

electrons. Under the influence of the electric field, the electrons accelerate toward the anode plane. At the anode wires just above the pad plane, the electrons reach energies sufficient to create an avalanche effect before being collected on the anode wires. The resulting positive ions induce a charge on the pad plane in the TPC that is proportional to the ionization [2]. The faces of the TPC each have 12 super-sectors with both inner and outer anode pads, which are arranged into planes (rows) with 13 rows in the inner sector and 32 in the outer sector, as shown in Figure 9. The charge collected on each pad is sorted into 512 time bins in the beam (or "z") direction, giving about 70 million samples total [6]. Note that the TPC is not able to detect tracks coming from particles of a neutral charge. In summary, the TPC provides information on each particle's

charge, momentum, and energy loss in the gas. The last of these is useful in determining the type of particle (PID).

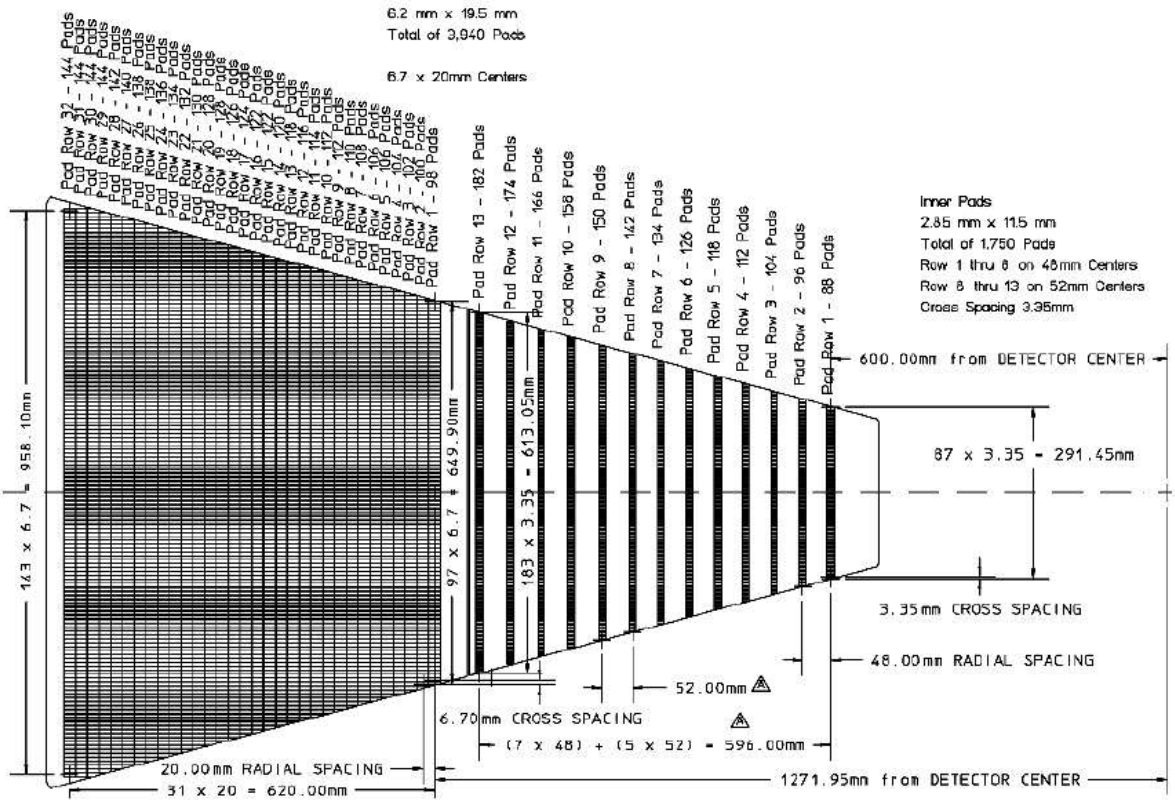

Figure 9: Anode Pads [8]

2.2.2. Trigger Detectors

RHIC provides about 2000 ion collisions per second; however, STAR can only record data at about 500 Hz and must, therefore, use specific trigger criteria. The Beam-Beam Counters (BBC), the Central Trigger Barrel (CTB), and the Zero-Degree Calorimeters (ZDCs) are some examples of the trigger detectors at STAR [6]. The CTB surrounds the TPC and uses photomultiplier tubes, in which light output is proportional to track multiplicity, in order to allow faster processing based upon the multiplicity of the event in question. The ZDCs measure

spectator neutrons resulting from the breakup of the nuclei since they are unaffected by the electric and magnetic fields. A high amount of spectator neutrons in both ZDCs acts as a trigger for events [6]. A trigger tells STAR and the TPC that an event has enough data to be worth recording.

2.2.3. Particle Reconstruction

Before the data can be analyzed by a STAR collaborator, all of the hits from the triggered events must be reconstructed into particle tracks. By using information collected by the TPC, particle tracks are identified as potential daughter particles. The term "daughter" indicates that these particles are actually the result of a decay of another particle. For example, a neutrally charged Λ particle will decay into a positively charged proton (p^+) and a negatively charged pion (π^-). This decay will occur on average 8 cm from the collision area and usually before the Λ enters the TPC. The paths and associated momenta of the charged daughters are detected by the TPC, and due to their charge and path curvature are classified as being either protons or pions. Next the mass of a proposed parent particle (a Λ in this case) is calculated from every combination of protons and pions for a given event. The mass of the candidate parent is calculated by the equation $M_\Lambda = M_p + M_\pi + 2(E_p E_\pi - \boldsymbol{p}_p \cdot \boldsymbol{p}_\pi)$, where M is the rest mass of a particle, E is the energy of a particle, and $\boldsymbol{p}$ is the momentum vector for a particle [3]. One count is added in the corresponding mass bin in a histogram of Λ mass, tallying the number of Λ candidates in different mass ranges.

2.2.4. Data Cuts

In the example given, many of the candidate parent particles (Λ's) in the mass histogram

are not true Λ's, resulting in an unwanted background. Consequently, the first step in analyzing the data is to conduct a cut study to optimize the levels at which data will be cut from the analysis. The goal while determining cuts is to keep as much of the signal as possible while reducing the maximum amount of noise for each of the three particles: Λ's, anti-Λ's, and K_S^0's. The majority of the cuts applied were geometrical, related to the paths of the daughter particles and determining if their paths would have allowed them to come from the same parent particle. After the cuts are applied, the mass peaks become much more defined. Residual background under the peak must still be determined. This is done through a process called sideband subtraction described later. After background is reduced, the peaks may be integrated to find the signal in each bin of transverse momentum.

2.2.5. Centrality

An additional parameter that is considered in the analysis of heavy-ion collisions is the centrality. Centrality is a measure of how much matter participates in a given collision. A collision that is "head-on" will have a higher centrality than one that is not. Centrality is measured by the number of particles produced in the detector for a given collision, also called the multiplicity [3]. When nuclei collide, the nucleons (protons and neutrons)

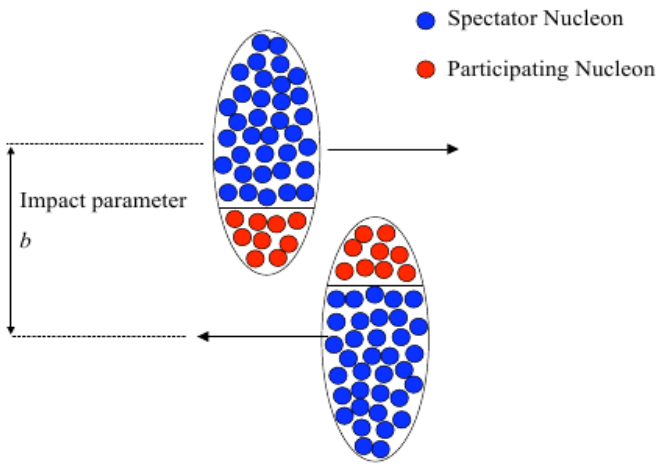

Figure 10: Centrality based on participating nucleons. [3]

that participate in the collision are called participating nucleons while those that pass by the collision area without colliding are called spectator nucleons [3]. Figure 10 illustrates spectator and participating nucleons through a picture of two nuclei colliding.

The data is analyzed by centrality, with 0-10% being the most central, 10-30% being less central, and 30-50% being the least central. Events with centrality lower than 50% were not used in this analysis. Contamination from pileup and low trigger efficiency make analysis difficult for those low centralities in this dataset. Determining the yield of strangeness for different centralities allows a study of the yield per event as a function of the number of participating nucleons (N_{part}), a parameter determined by centrality via a Glauber calculation [3]. Glauber theory gives an estimate of the number of participating nucleons if certain assumptions are made [3]. One assumption is that the collision is the superposition of many nucleon on nucleon collisions [3]. Others are that the nuclei travel in straight lines and that the matter in the nucleus follows a Woods-Saxon distribution [3]. Since collisions with a higher centrality have more participating nucleons, these collisions are expected to have higher yields of strangeness and a higher anti-baryon to baryon ratio.

Chapter 3 – Analysis of Copper Nuclei Collisions at 22 GeV

This chapter will begin by giving a summary of the data being analyzed and the process used to take the STAR data and turn it into meaningful measurements and graphs. It then describes the process by which the centrality groups are determined for the data, providing a view of the number of events in each range of multiplicity. Next, it shows the mass histograms containing all candidates for each of the parent particles: Λ's, anti-Λ's, and K_S^0's. After demonstrating the need to eliminate background, the cuts on the parent particles are explained. Finally, the mass histograms of the parent particles are shown after all cuts are applied.

3.1 Dataset Summary

The data examined in this analysis was collected by STAR in 2005 from two Cu beams colliding at a center-of-mass energy of 22 GeV per nucleon. Information for 3,517,551 events is contained in this dataset. While 22 GeV is an extremely high energy, it is actually a relatively low energy for RHIC compared to other data collected by STAR. When the data is supplied by STAR, it comes in the form of "trees" that can then be analyzed using C++ code. This project utilized a programming framework called ROOT, which is a C++ based set of libraries designed for particle physics analysis. C++ code is used in conjunction with ROOT to generate histograms and graphs of different properties of reconstructed particles and other event components. Cuts on the data based on different parameters are implemented within the code.

3.2 Centrality Determination

The analyzed events are grouped into three different windows of centrality: 0-10%, 10-30%, and 30-50%. No events with 50-100% centrality, the events with the least centrality and lowest numbers of participating nuclei, were used in the analysis. In order to determine the events falling into each region of centrality, a histogram was generated showing the number of events for each bin of multiplicity as seen in Figure 11. Events with the highest reference

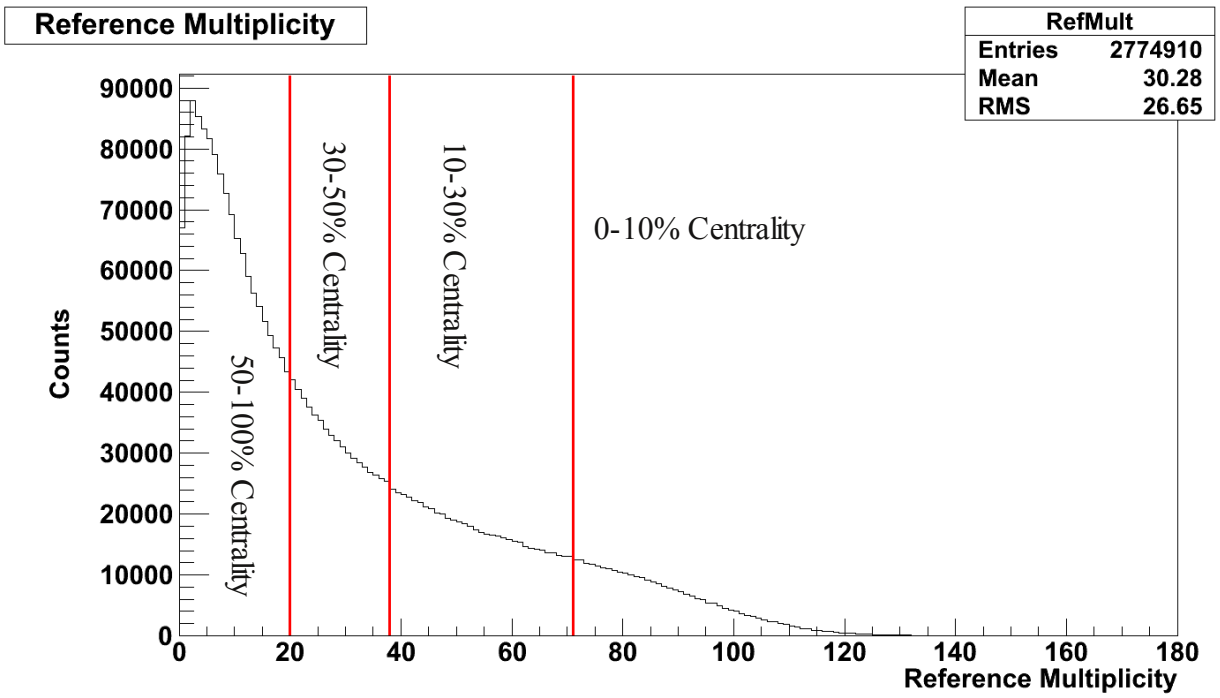

Figure 11: Reference Multiplicity Histogram

multiplicities are the most central events. This curve was integrated to determine the number of events in the reference multiplicity histogram to be 2,774,910. The 10% of those events with the highest reference multiplicity (greater than 71) represent the 0 to 10% centrality. The next 20% (reference multiplicity between 38 and 71) represent the 10-30% centrality and the last 20% (reference multiplicity between 20 and 38) represent the 30-50% centrality. These regions are shown in Figure 11. The red lines in the graph delineate the three regions of centrality.

3.3 Mass Distributions

The mass distribution containing all possible candidate parent particles and their masses are shown for Λ's in Figure 12, Anti-Λ's in Figure 13, and K_S^0's in Figure 14. The signal can be seen as a peak sitting on a significant background. These examples are shown for the highest centrality events (0-10%). Similar histograms were generated for the other two centrality regions as well (10-30% and 30-50%).

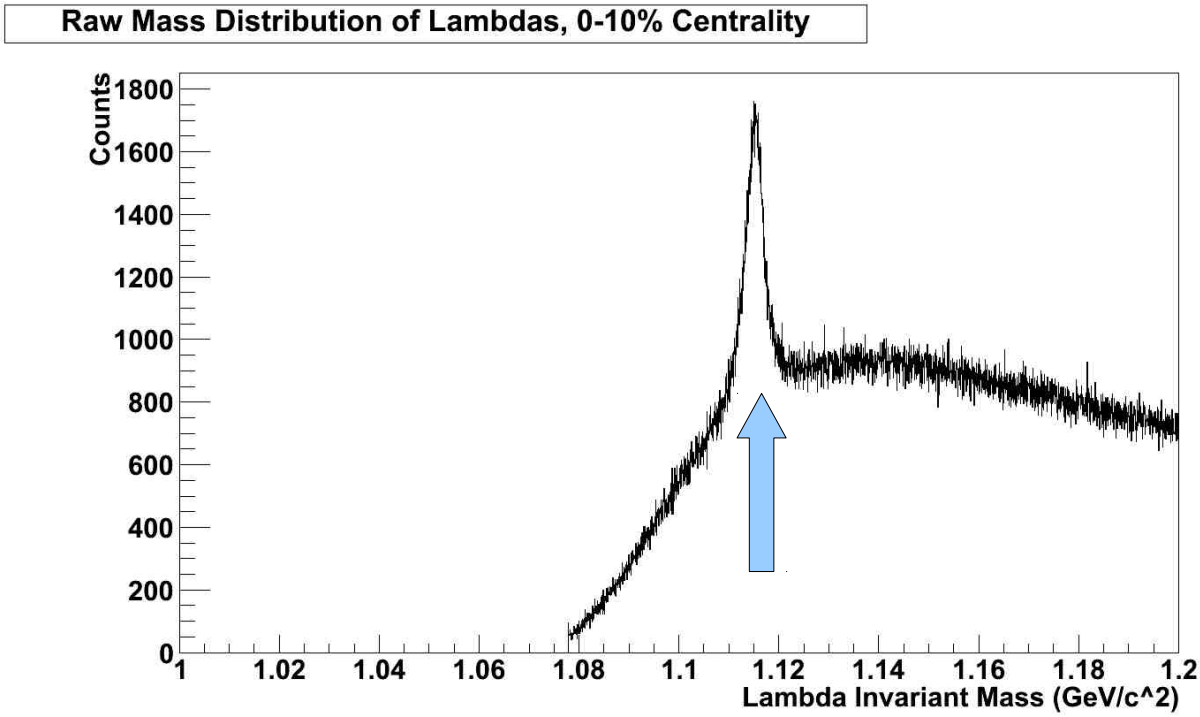

Figure 12: Raw Mass Distribution Histogram of Lambda Candidates, 0-10% Centrality

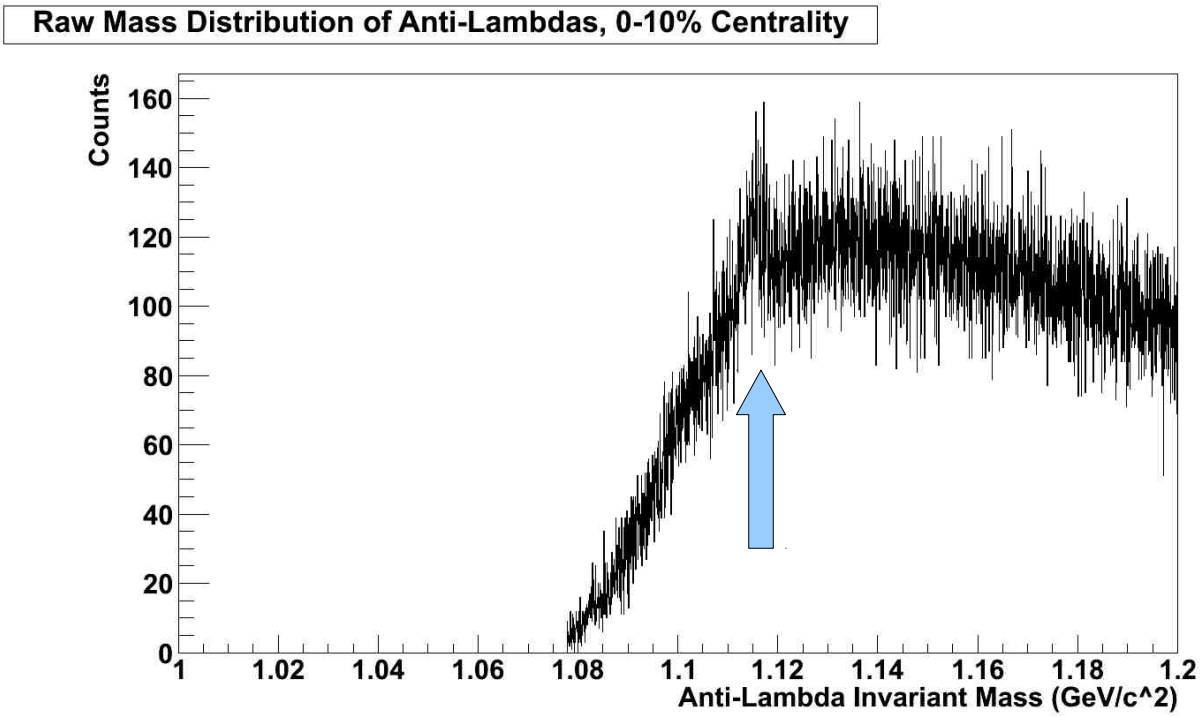

Figure 13: Raw Mass Distribution Histogram of Anti-Lambda Candidates, 0-10% Centrality

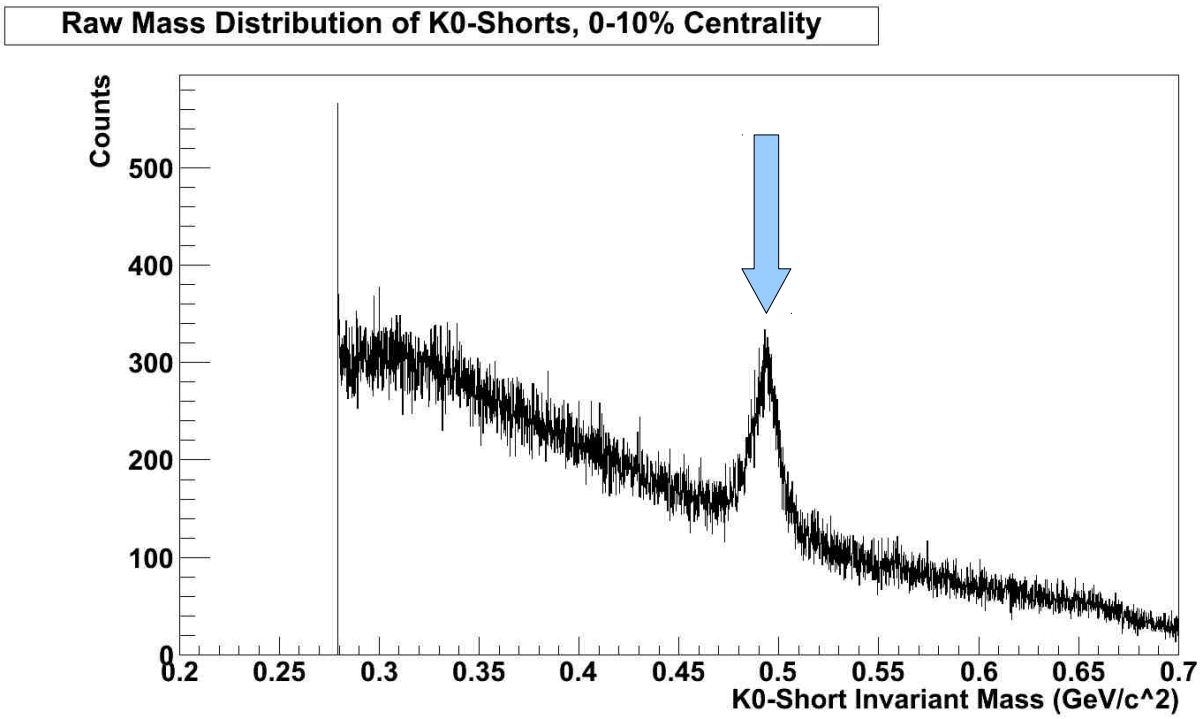

Figure 14: Raw Mass Distribution Histogram of K0-Short Candidates, 0-10% Centrality

3.4 Quality Cuts

In order to reduce the background in the mass distribution histograms, cuts were placed on the tracks in order to reduce the number of false Λ, Anti-Λ, and K_S^0 candidates. The goal is to provide the most signal for the least amount of background. Cuts were made on the geometric properties of the tracks, specifically on the decay length of the proposed parent particle, the distance of closest approach (DCA) of the proposed parent particle to the primary vertex of the collision, and the DCA of the daughter particles to each other and to the primary vertex. These cuts are best illustrated with the aid of Figure 15.

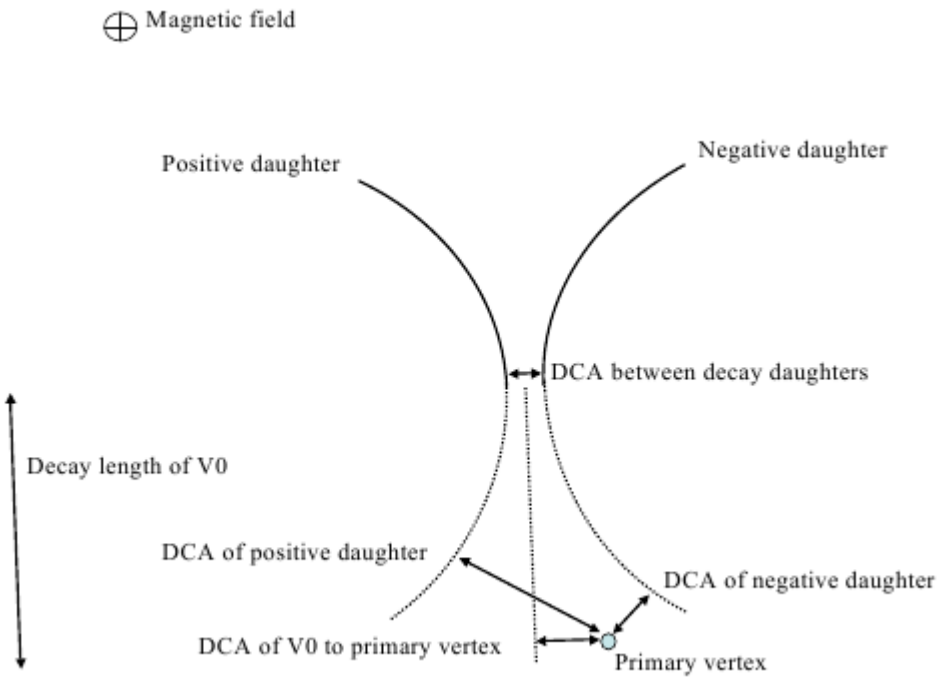

Figure 15: Event Geometry Pertinent to Cuts [3]

3.4.1 Decay Length

The term V0 refers to a particle of neutral charge that decays into two charged particles, which will travel in different directions if a magnetic field is present [3]. The "V" stands for vertex, and the "0" refers to the fact that it is a neutral decay. Since the TPC can only detect charged particles, it will only detect the daughters of a V0 candidate; therefore, information about the V0s must be determined solely from their daughters. The decay length is the distance that the V0 travels from the primary vertex of the collision before it decays into its daughters. The primary vertex is the point of collision for the event, determined by finding the point of intersection of charged tracks. Some of the background in the raw mass histograms is caused by accepting a V0 candidate with a decay length that is too small. To remove some of this background, any Λ, anti-Λ, or K_S^0 candidates with a decay length less than 8 cm were cut. Figures 16, 17, and 18 show the decay length for Λ's, anti-Λ's, or K_S^0's versus their invariant mass. Candidates below the red line were removed from the mass histograms. The blank region on the graphs is due to online cuts applied before the analysis. For these two-dimensional histograms, the colors nearest red on the spectrum represent more candidates found with a given mass and decay length while the colors nearest blue signify less candidates found with those two characteristics. These examples are for 10-30% centrality, but the same cuts were applied in the other two centralities as well.

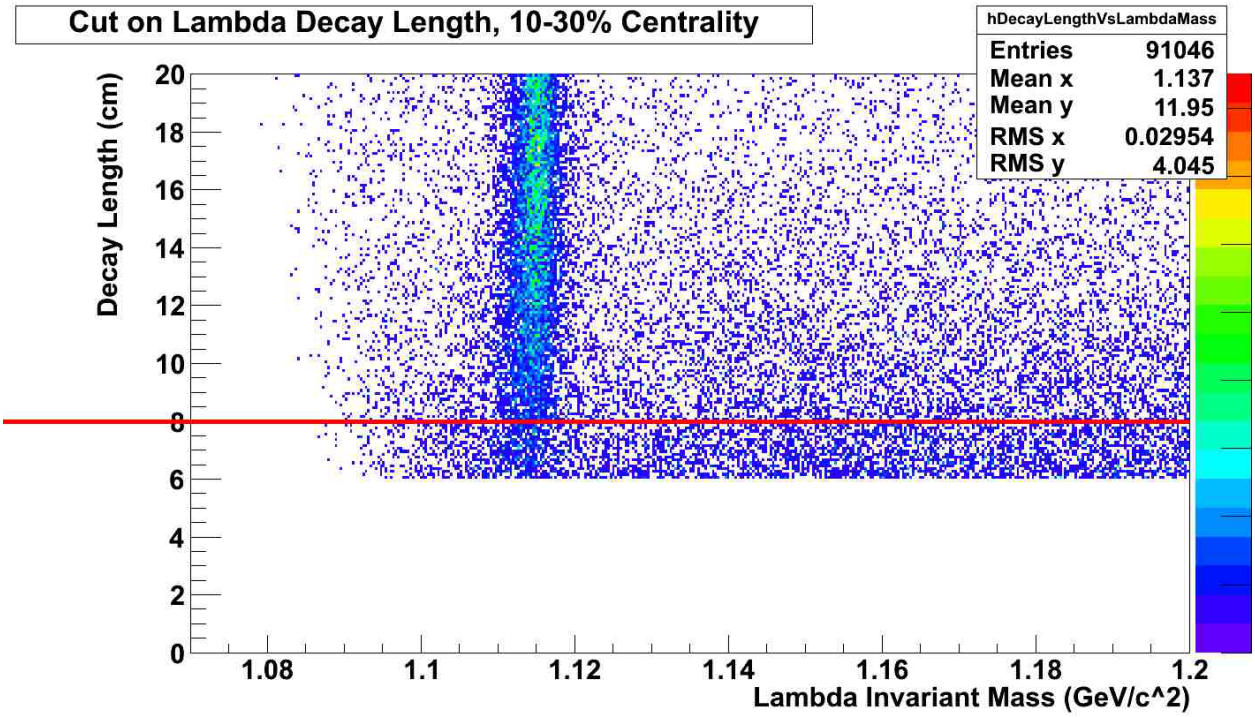

Figure 16: Cut on Lambda Candidate Decay Length, 10-30% Centrality

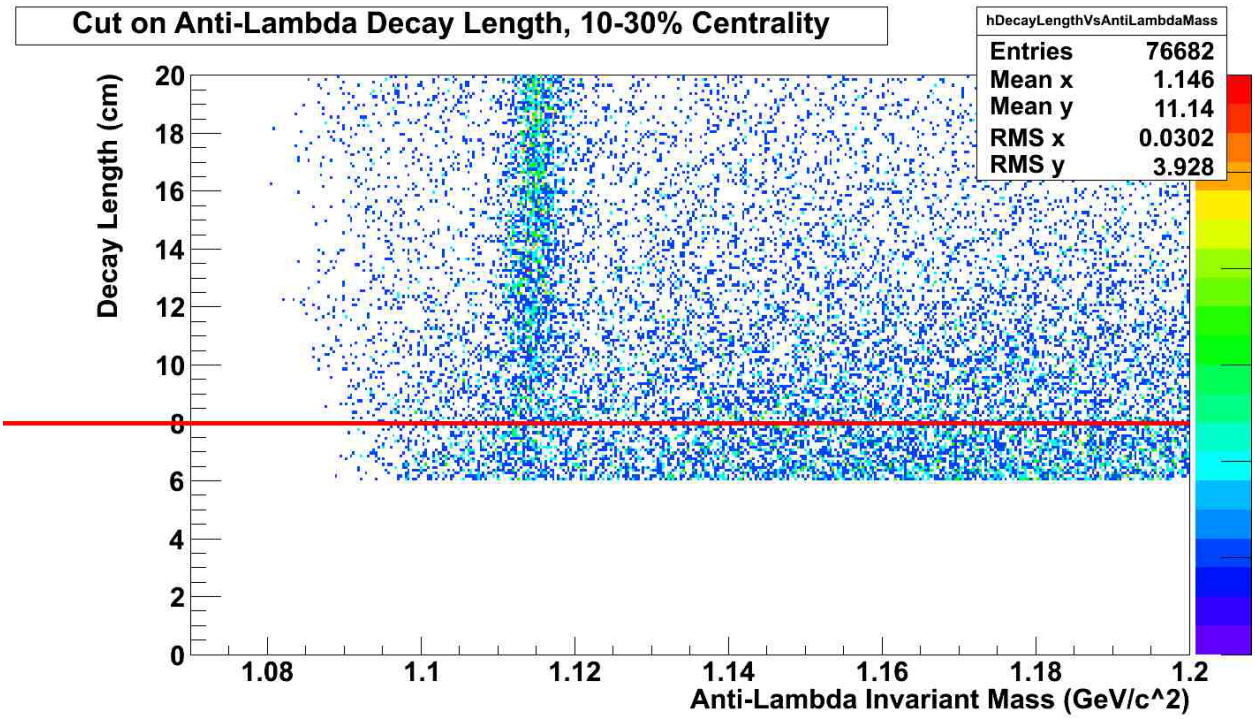

Figure 17: Cut on Anti-Lambda Candidate Decay Length, 10-30% Centrality

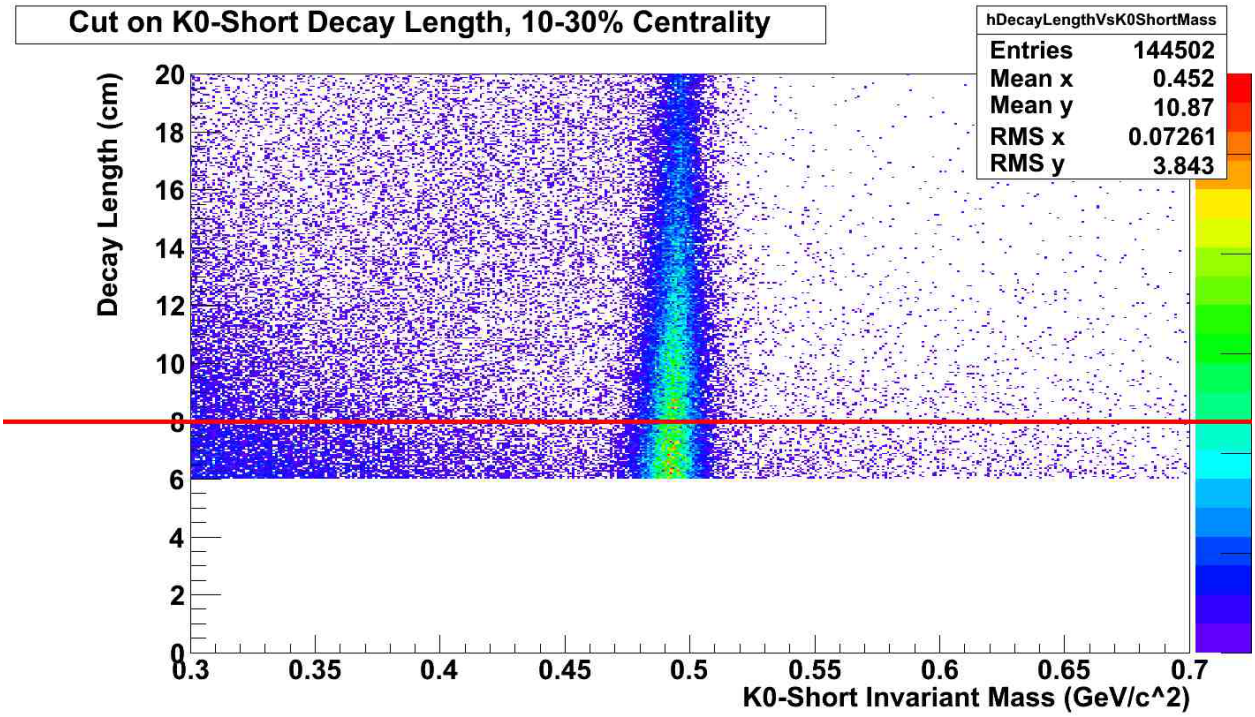

Figure 18: Cut on K0-Short Candidate Decay Length, 10-30% Centrality

3.4.2 DCA V0 to Primary Vertex

For every possible pair of daughters, STAR software constructs the path that the parent V0 would have taken, shown as a dotted line in Figure 15, considering the curvature of the daughter tracks as well as the mass of the daughter particles. The closest distance that this neutral particle's straight track comes to the primary vertex of the collision is called the DCA to the primary vertex, shown in Figure 15. For Λ's and Anti-Λi's, any DCA of the V0 to the primary vertex greater than 0.5 cm was cut. For K_S^0's, this cut was applied at 0.6 cm. The cuts are demonstrated in Figures 19, 20, and 21. Again, the examples come from the 10-30% centrality region.

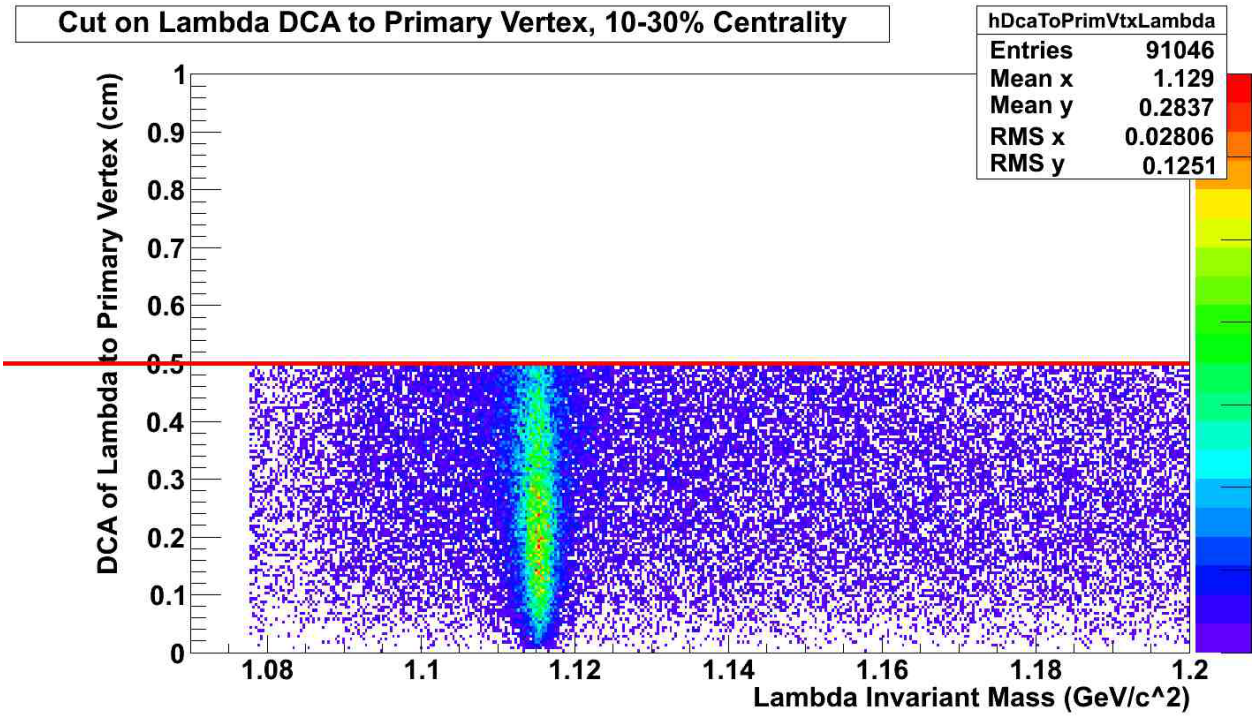

Figure 19: Cut on Lambda DCA to Primary Vertex, 10-30% Centrality

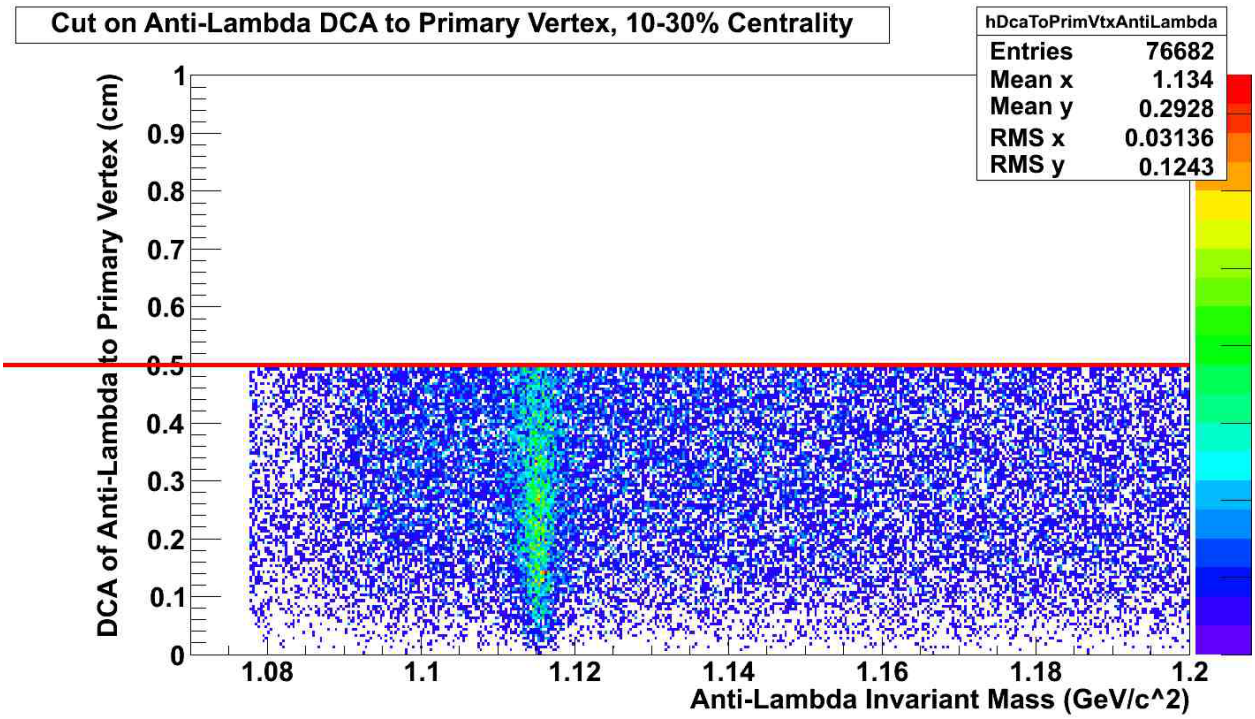

Figure 20: Cut on Anti-Lambda DCA to Primary Vertex, 10-30% Centrality

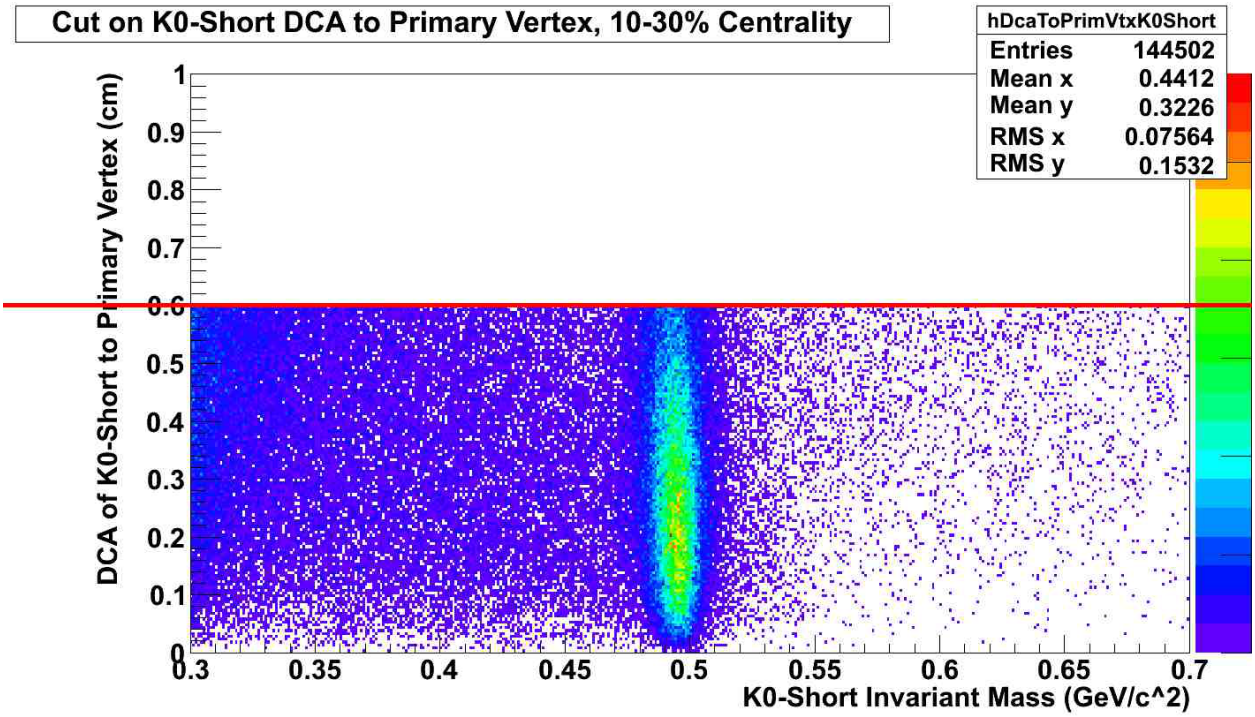

Figure 21: Cut on K0-Short DCA to Primary Vertex, 10-30% Centrality

3.4.3 DCA Daughters to Primary Vertex

Each daughter track that is detected by STAR has an associated interpolated track outside of the instrumented region of the experimental setup that is determined based on its curvature in the detected part of its track. If this interpolated track does not pass close enough to the primary vertex, it can be cut since it is less likely that this daughter particle detected actually resulted from a true V0 parent decay. This cut was applied separately to the positively and negatively charged daughters that were detected. For Λ's, the cut was applied with a maximum allowed DCA of 1.05 cm for the positive daughter and 2.5 cm for the negative daughter. For Anti-Λ's, this was reversed since the daughter of an anti-matter particle has the same characteristics as the daughter of its corresponding matter particle with the opposite charge. Thus, there was a maximum allowed DCA of 2.5 cm for the positive daughter and 1.05 cm for the negative daughter. For K_S^0's, the maximum allowed DCA was 1.3 cm for both the positive and negative

daughters. Figures 22, 23, 24, and 25 show this cut for the positive and negative daughters of Λ's and K_S^0's at 10-30% centrality.

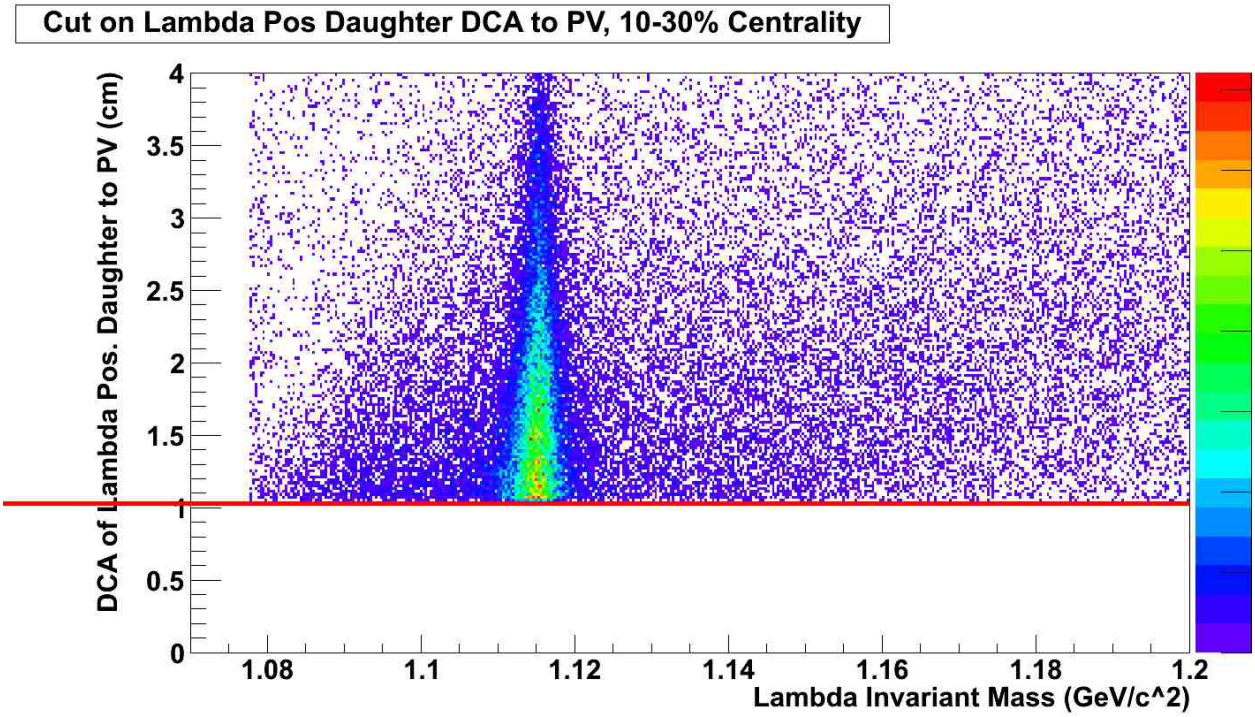

Figure 22: Cut on Lambda Positive Daughter DCA to Primary Vertex, 10-30% Centrality

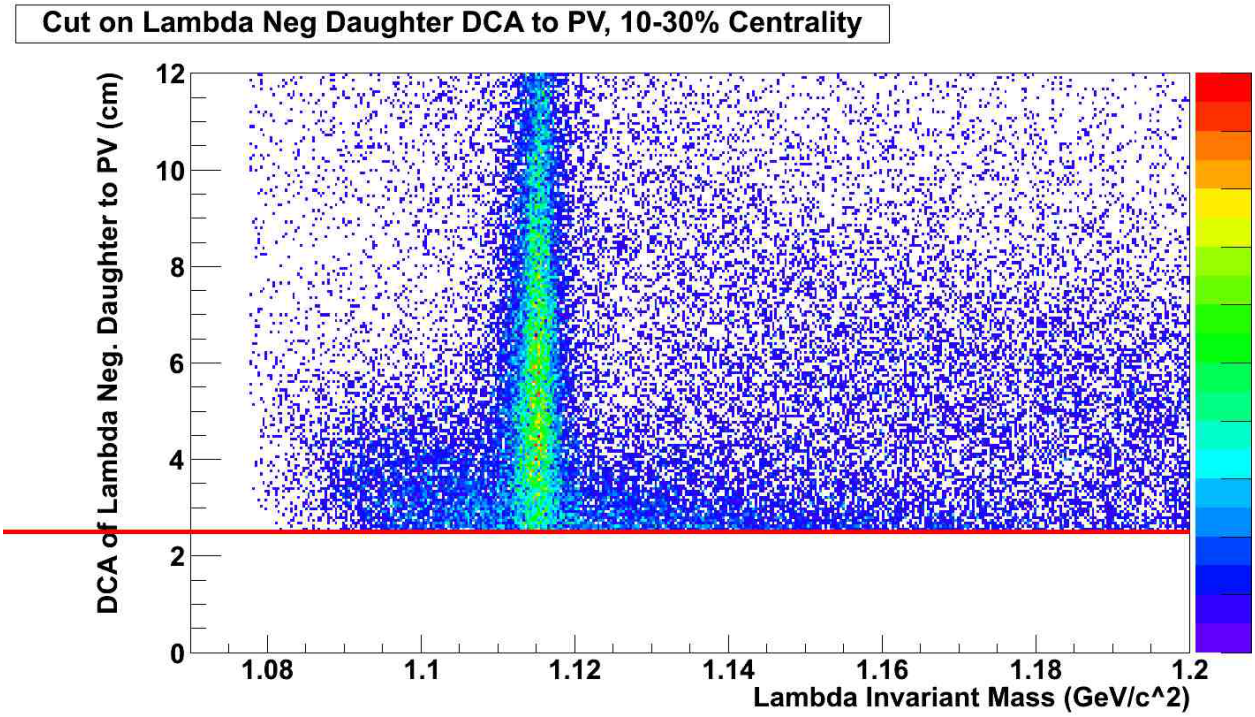

Figure 23: Cut on Lambda Negative Daughter DCA to Primary Vertex, 10-30% Centrality

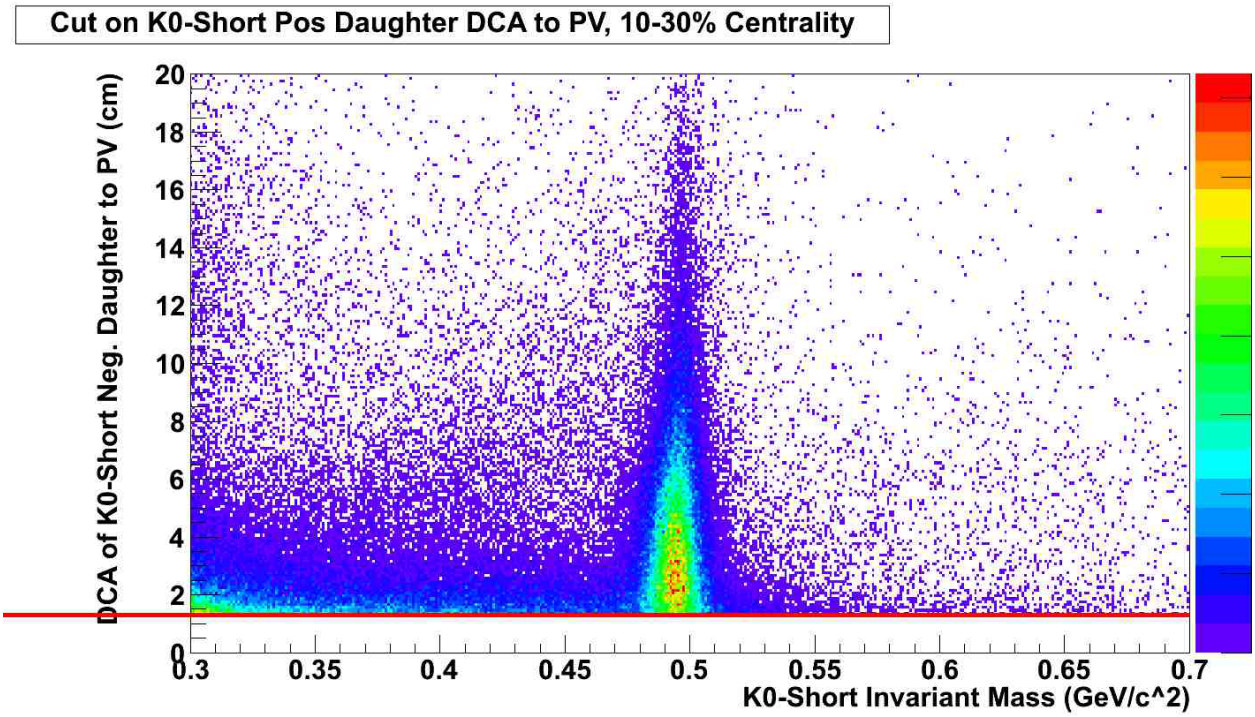

Figure 24: Cut on K0-Short Positive Daughter DCA to Primary Vertex, 10-30% Centrality

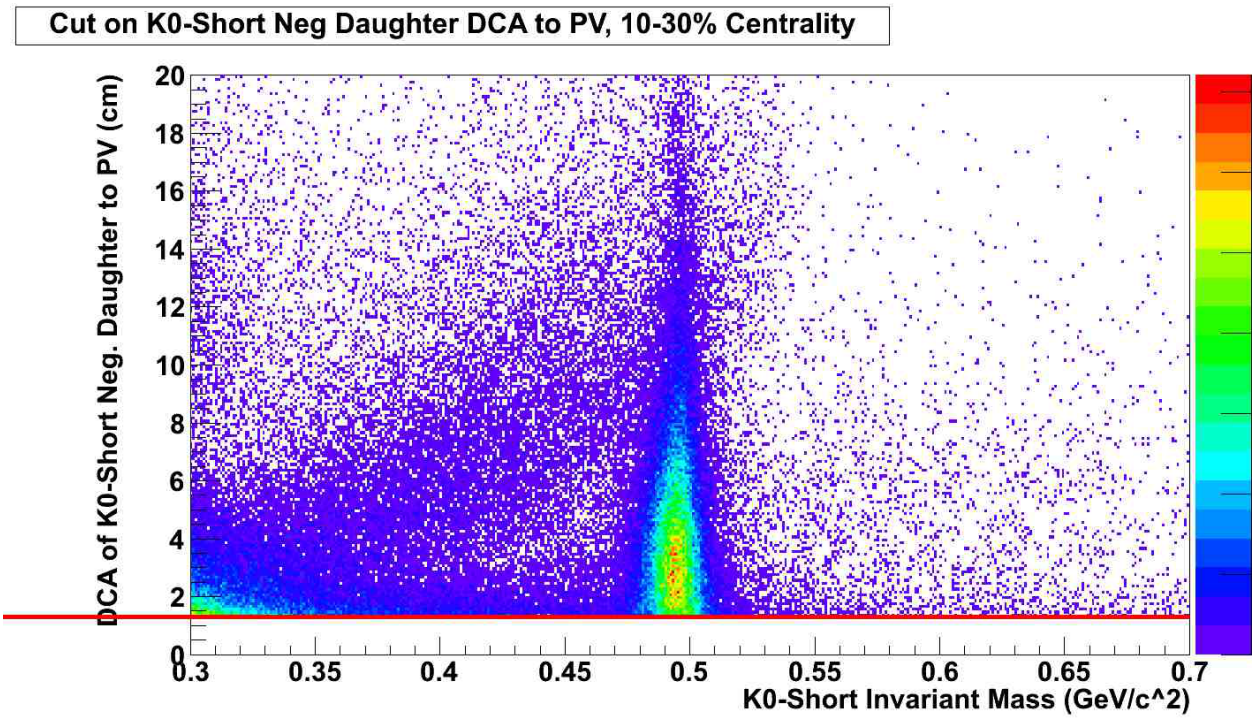

Figure 25: Cut on K0-Short Negative Daughter DCA to Primary Vertex, 10-30% Centrality

3.4.4 DCA Daughters

One last important geometrical cut is based on the closest distance that the two daughter particles come to one another. If their interpolated tracks never come close to one another, it is safe to say that the two daughter particles did not come from the same parent. This cut on the DCA of the V0 daughters was applied at 0.8 cm for Λ's, Anti-Λ's, and K_S^0's. The cuts can be seen in Figures 26, 27, and 28 for Λ's, Anti-$\Lambda i's$, and K_S^0's at 10-30% centrality.

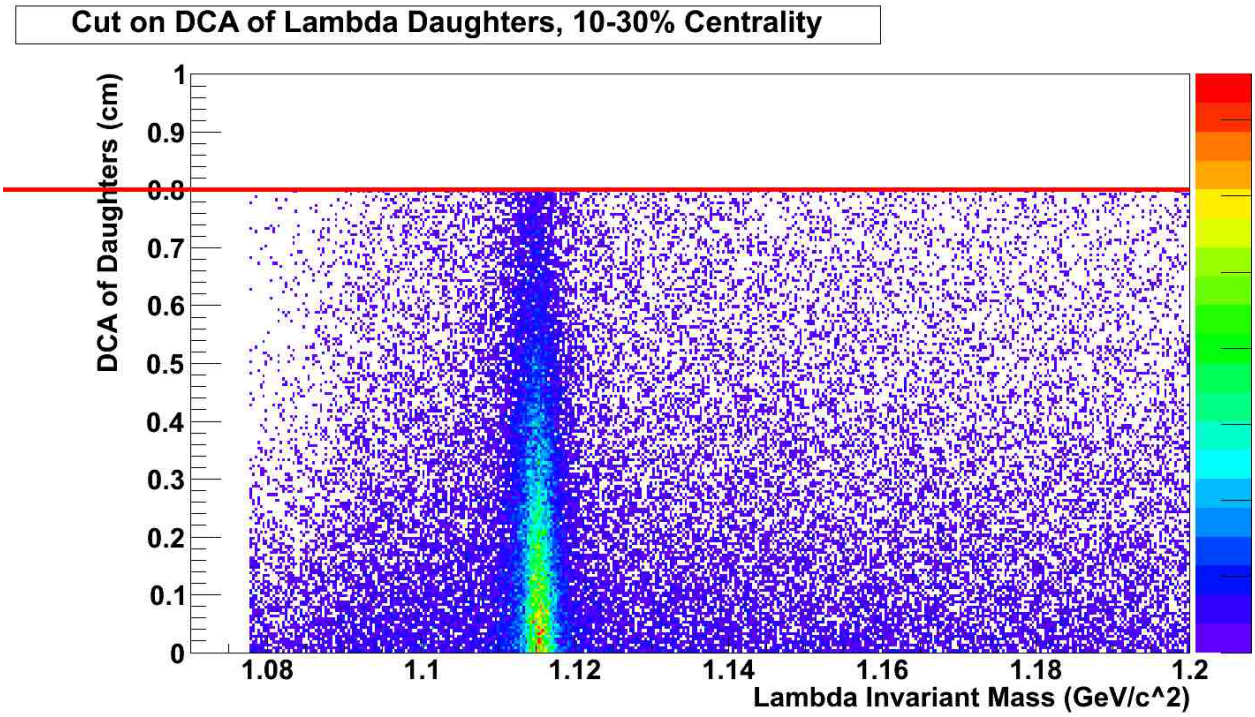

Figure 26: Cut on DCA of Lambda Daughters, 10-30% Centrality

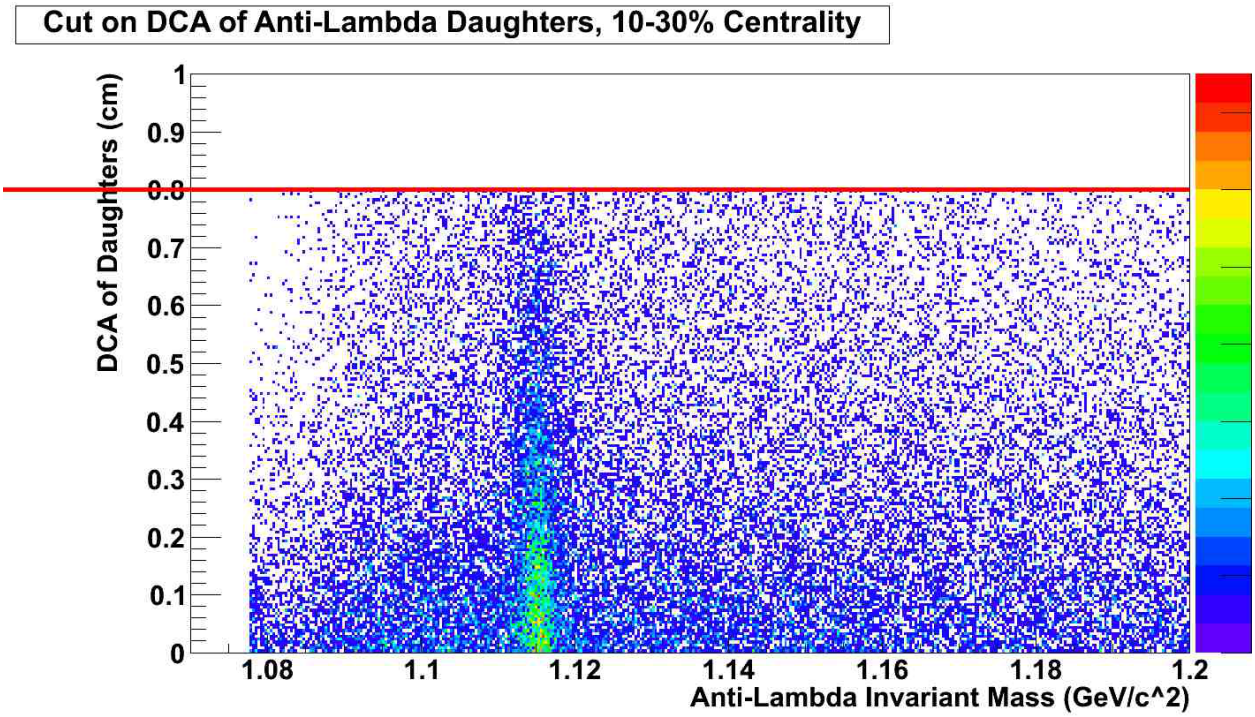

Figure 27: Cut on DCA of Anti-Lambda Daughters, 10-30% Centrality

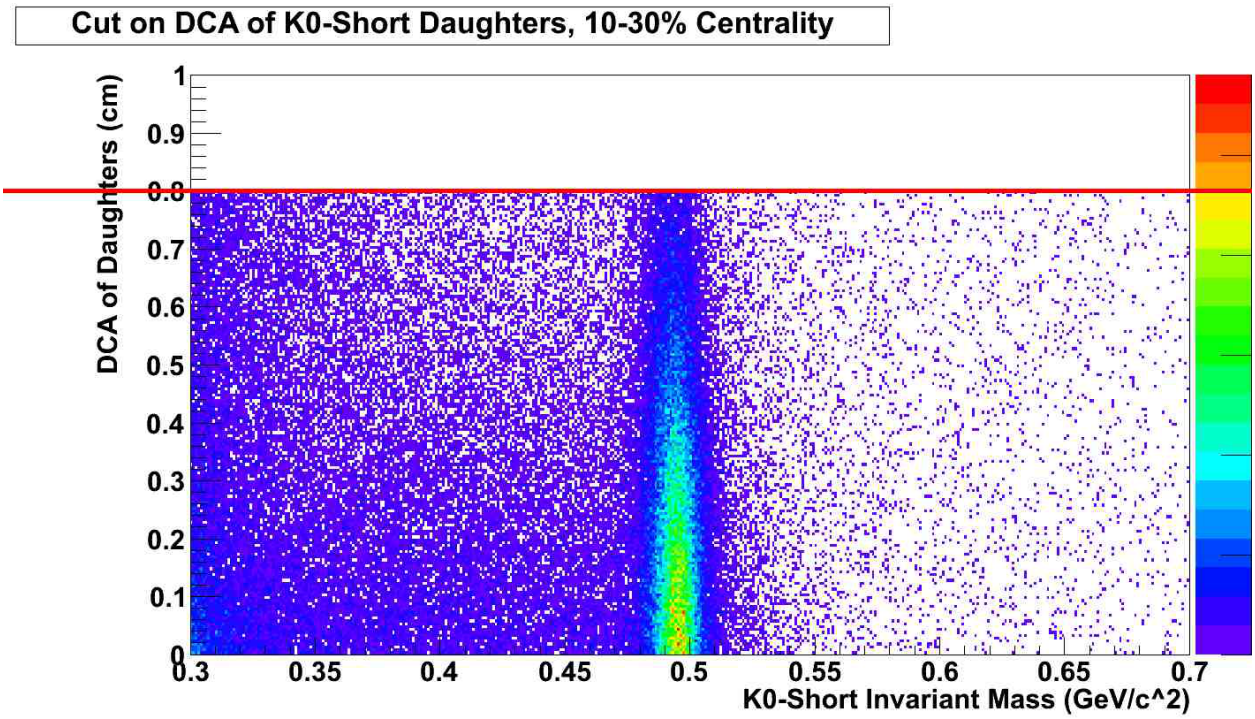

Figure 28: Cut on DCA of K0-Short Daughters, 10-30% Centrality

3.4.5 Rapidity

Rapidity is a quantity that describes the relativistic velocity of particles in an event [3]. It is a quantity that can be added, unlike relativistic velocities. It is especially helpful when comparing data from colliders to data from fixed target experiments [3]. In this analysis, the cut on rapidity for an event was set to the calibration parameters of the TPC, where the absolute value of the rapidity must be 0.5 or less. The TPC has its greatest efficiency and most symmetric acceptance in this range.

3.4.6 Number of Hits

The number of hits on the TPC detector for a given track can be helpful in identifying which tracks are real and which were reconstructed incorrectly. For this analysis, the minimum number of hits for a positive or negative daughter track for any V0 to be accepted is 15. This will provide long, high-quality tracks with the best determined characteristics.

3.4.7 Sideband Subtraction

The process by which residual background is removed from under the mass peak is called sideband subtraction. In this process, the average height of the noise surrounding the signal is subtracted from the signal itself. Figure 29 is an example of a signal of Anti-Λ counts in a histogram for invariant mass. This

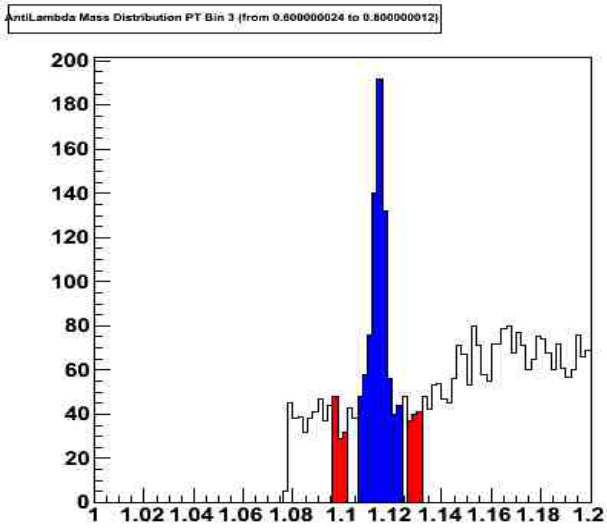

Figure 29: Sideband Subtraction for Anti-Lambdas at 10-30% Centrality from 0.6-0.8 GeV/c Momentum Bin

histogram is for a particular region of Anti-Λ momentum, between 0.6 and 0.8 GeV/c, and at 10-30% centrality. Since the red sidebands on either side of the peak may differ in magnitude, the average of the two red bands is subtracted from the blue signal to account for the residual background under the peak.

3.5 Candidates After Cuts

Finally, after all of the cuts have been applied, the mass peaks for each V0 can be integrated to determine the total yield. The mass peaks for Λ's, Anti-Λ's, and K_S^0's after cuts in the 0-10% centrality region are shown in Figures 30, 31, and 32. When compared with Figures 12, 13, and 14, the effects of the cuts are made obvious. The signal peaks are much more defined now and are ready for analysis of the physics involved in the collision. After signal integration and sideband subtraction, acceptance and efficiency corrections must be applied to the data. The actual mass for the Λ's and Anti-Λ's is 1.12 GeV/c^2, and that for the K_S^0's is 0.50 GeV/c^2.

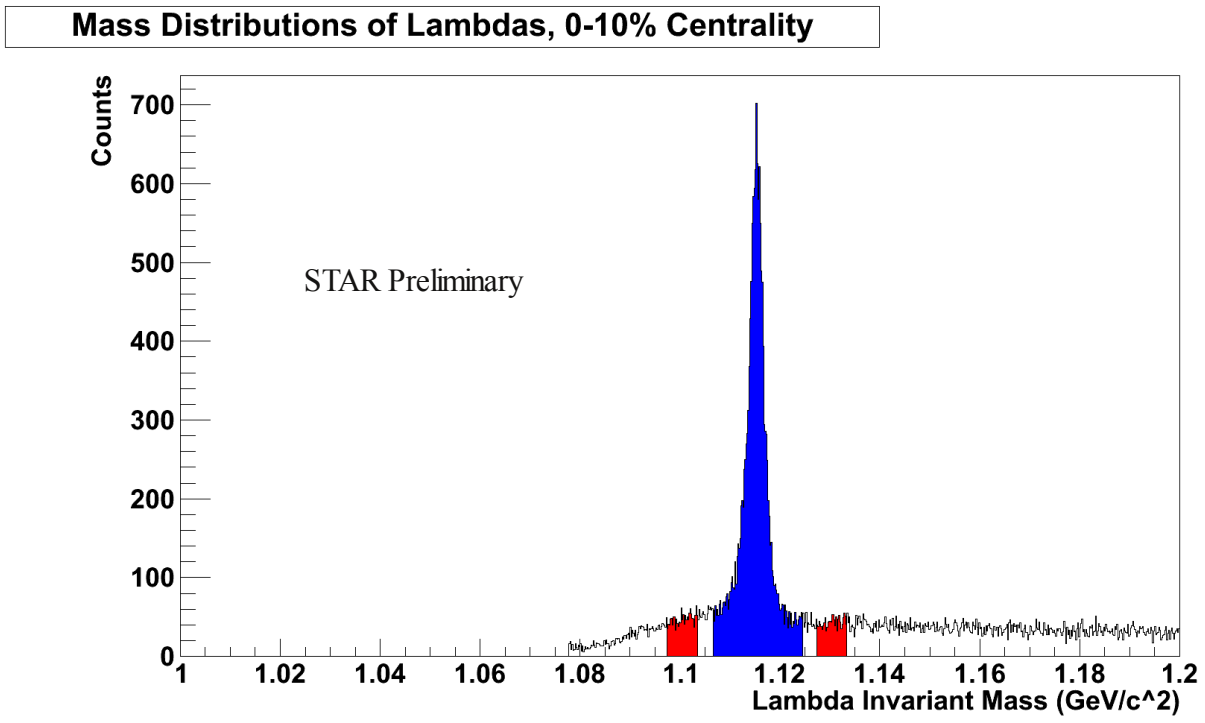

Figure 30: Mass Distribution of Lambdas After Cuts, 0-10% Centrality

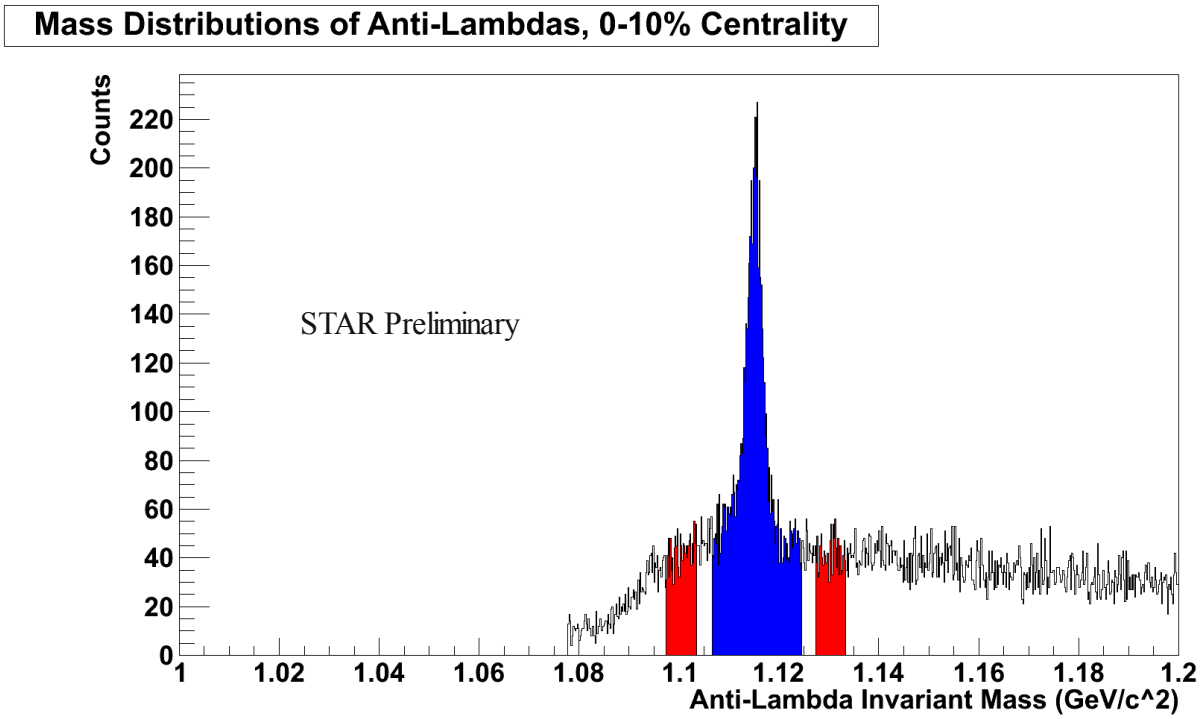

Figure 31: Mass Distribution of Anti-Lambdas After Cuts, 0-10% Centrality

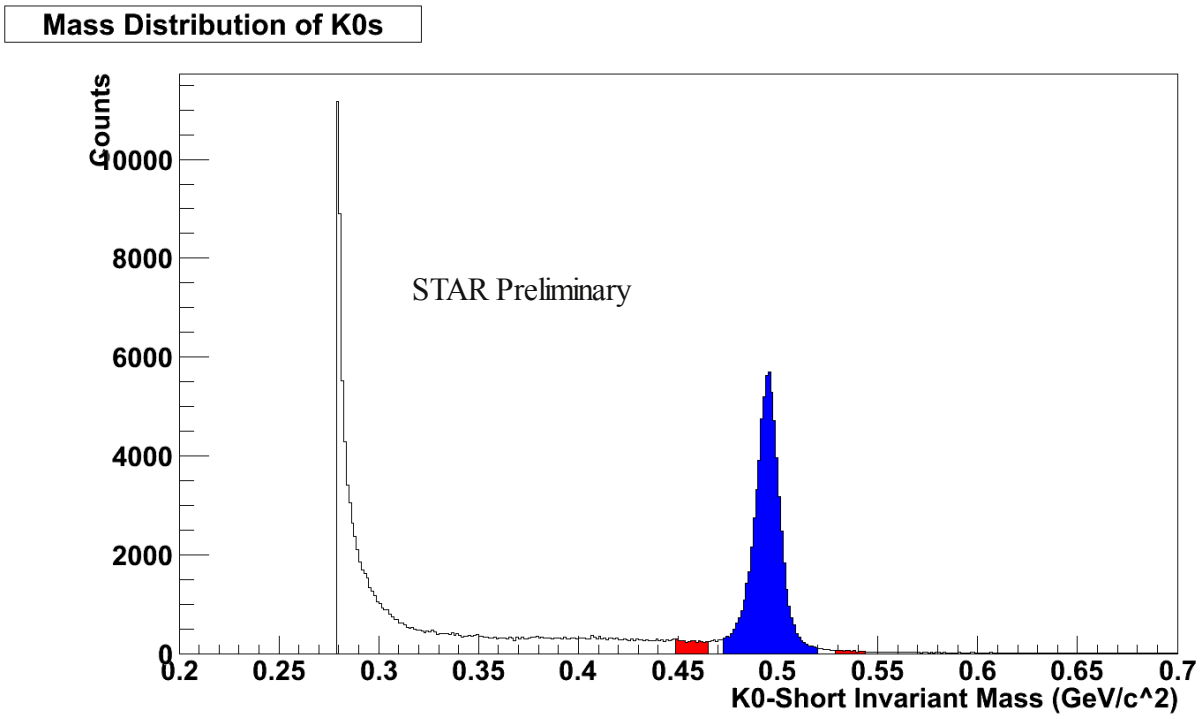

Figure 32: Mass Distribution of K0-Shorts After Cuts, 0-10% Centrality

Chapter 4 – Efficiency and Acceptance Corrections

Before the data can be used to make conclusions about the physics of the collision, it must first be corrected to account for finite detector size and reconstruction inefficiency. The efficiency and acceptance corrections are determined with the help of a software simulation called GEANT. Once the corrections are applied to the data, the corrected yield of events in different regions of momentum can be determined.

4.1 GEANT Simulation

Acceptance and efficiency corrections are applied to the data to account for the fact that the cuts on the data will potentially cut an actual parent V0 and leave some false V0 candidates in the statistics. Additionally, some parent tracks will be lost because the detector itself is finite and has a hole through the middle. Other tracks will be lost due to the fact that the tracking software is not perfect in its reconstruction. To remedy these effects, a program called GEANT is used in a software simulation of the collision [3]. In a process called the embedding chain, simulated V0s are embedded into the data that was physically collected from STAR at the signal level [3]. In other words, additional simulated data is combined with the data collected at the physical accelerator at STAR. Now, the same cuts are placed on the entire set of data as before, and the event is processed with the usual reconstruction chain of software. By determining how many of the simulated parents are eliminated by the cuts or lost from the detector altogether, a

correction is placed on the data to account for the actual parents that were eliminated by the cuts.

4.2 Correction Application

The mass distributions for candidates of Λ's, anti-Λ's, and K_S^0's were divided into specific bins, or windows, of momenta. This was done for each of the three centrality regions. A mass distribution for each candidate particle was created for each of 15 bins of momentum. The peak of each of these distributions was integrated and the residual background subtracted to give the total yield of particles for an event at a given momentum. The corrections are applied by dividing the yield of each momentum bin by its corresponding correction factor C, where C = (N_R/N_G) [3]. N_R is the number of simulated V0s found in the analysis. N_G is the total number of V0s generated by GEANT and put into the events. BR is the branching ratio, which statistically accounts for the Λ's that decay into uncharged particles and cannot be detected by STAR. When the yield for each momentum bin is divided by the correction factor, the corrected yield for each

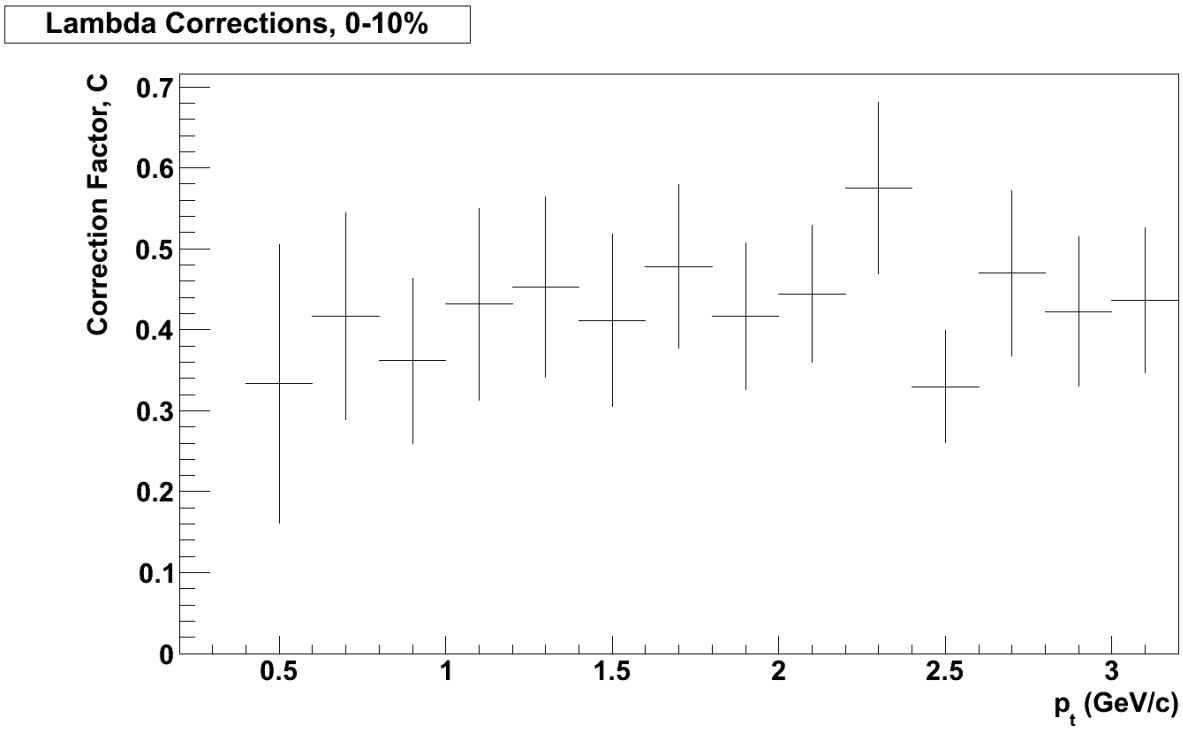

Figure 33: Lambda Correction Factors, 0-10% Centrality

momentum bin is obtained. The correction factors for Λ's, anti-Λ's, and K_S^0's in the 0-10% centrality are shown in Figures 33, 34, and 35.

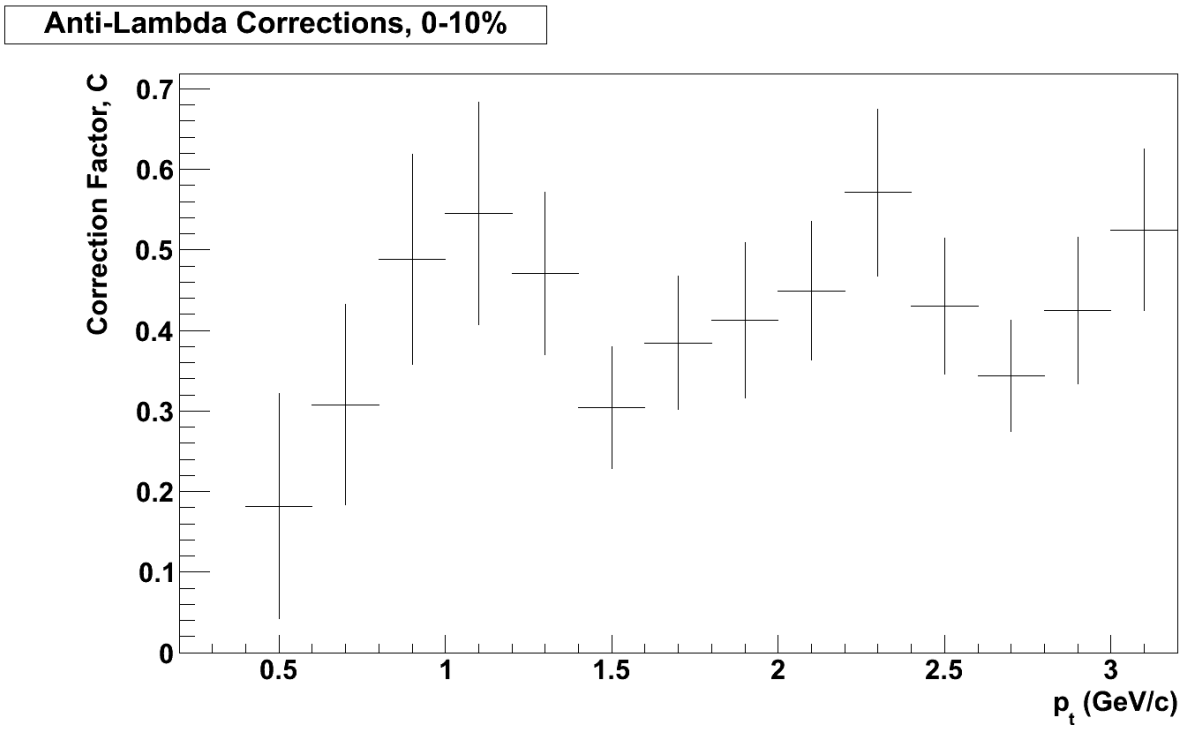

Figure 34: Anti-Lambda Correction Factors 0-10% Centrality

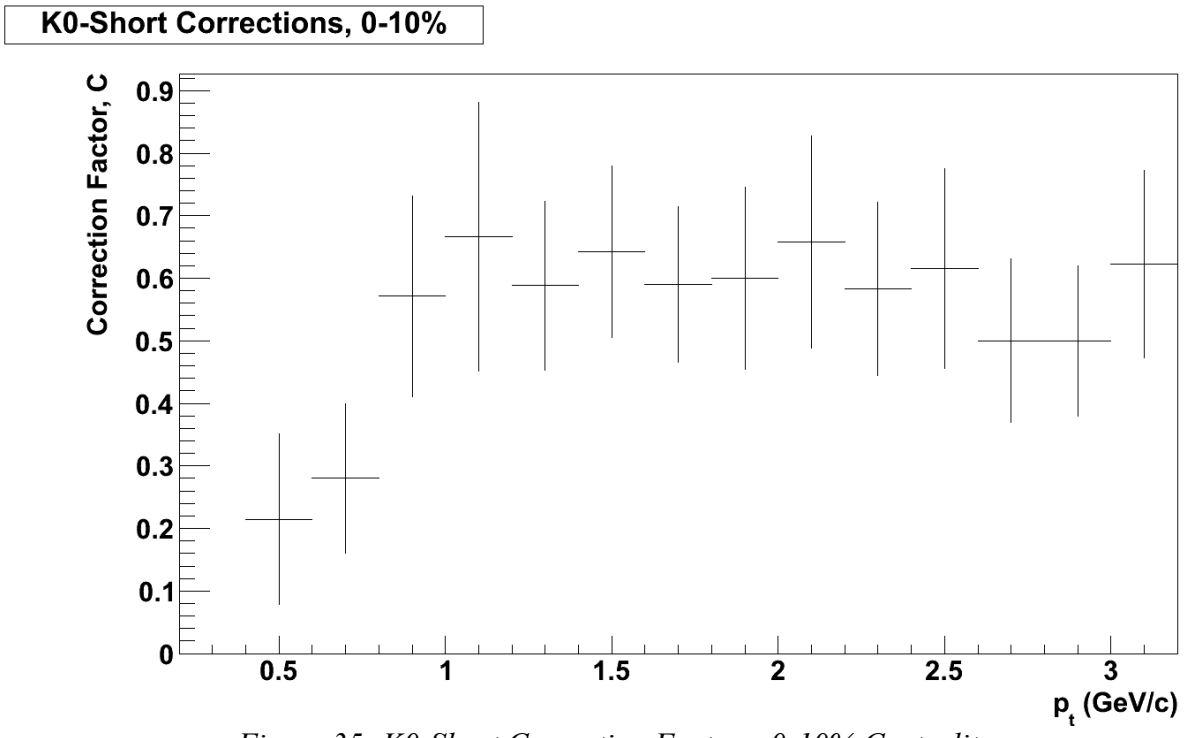

Figure 35: K0-Short Correction Factors, 0-10% Centrality

4.3 Corrected Transverse Momentum Spectra

The momentum bins described above are shown in Figure 36, which shows 15 different momentum bins along with their mass peaks. The part of the distribution in blue was integrated to find the yield for that particular momentum bin. The parts of the distribution in red were subtracted from the parts in blue in the sideband subtraction procedure described previously. Transverse momentum (p_t) is momentum that is perpendicular to the direction of the beam. It is of interest because p_t cannot come from the momentum of the beam, but somehow from the energy in the collision area.

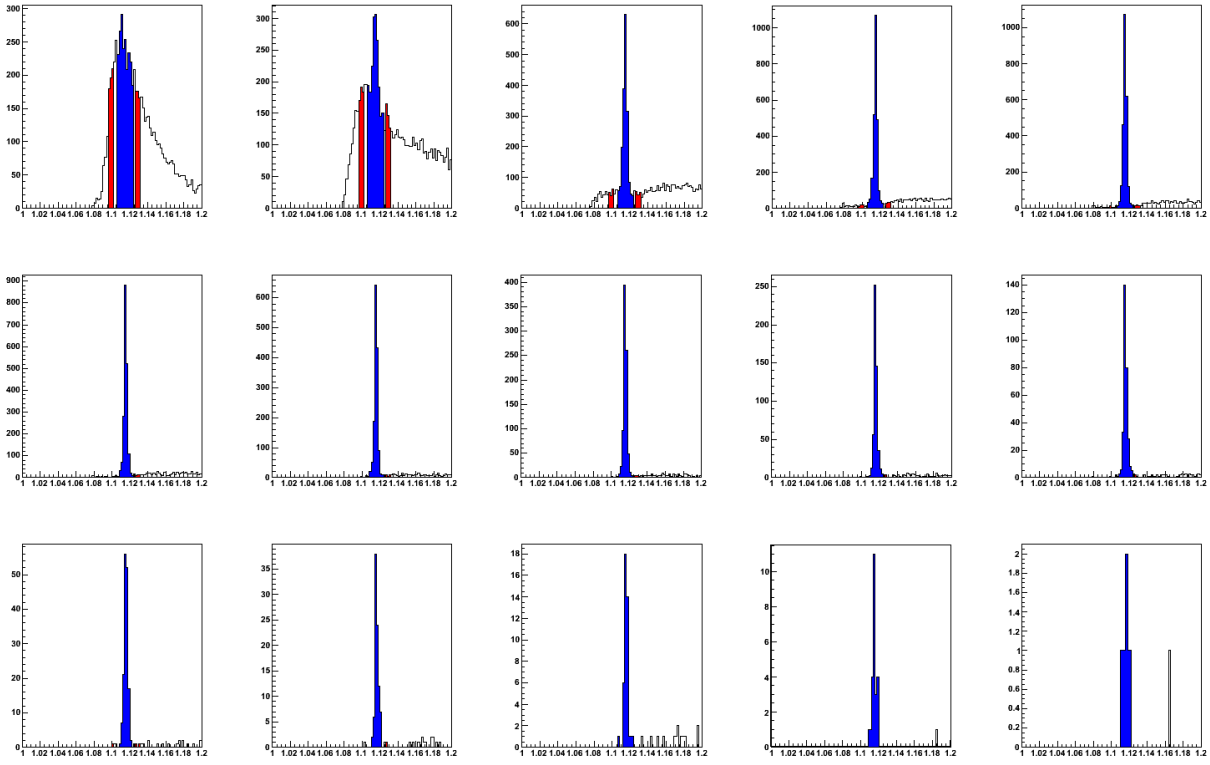

Figure 36: Mass Peaks by Momentum Bin for Lambdas, 0-10% Centrality

The momentum bins cover the range between 0.2 and 3.2 GeV/c in increments of 0.2 GeV/c, reading the histograms from left to right, top to bottom. In the example shown above with the Λ's, the first two bins are thrown out due to excess background that makes the signal unreliable

as a data point. The last bin is thrown out because of minimum statistics, only two counts total. Each of these momentum bins, once corrected by the correction factor, becomes one point on a plot of yield vs. transverse momentum, shown in Figures 37, 38, and 39 on a logarithmic y-axis. The red lines indicate a Boltzmann Distribution that was fitted to the data points using ROOT. The Boltzmann Distribution fit treats the system as a thermal model. The fits were integrated from zero to infinity to determine the overall yield per event (dN/dy) for the respective particle. The average transverse momentum is documented as $\langle p_T \rangle$. The Boltzmann fit is shown with inverse slope parameter *T*. The examples shown are for 0-10% centrality.

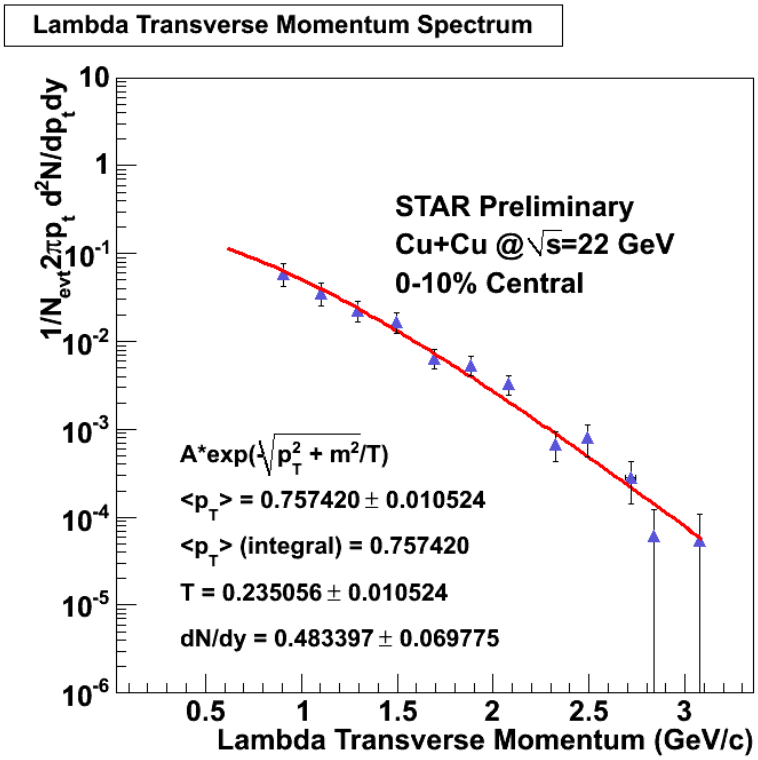

Figure 37: Lambda Transverse Momentum Spectrum, 0-10% Centrality

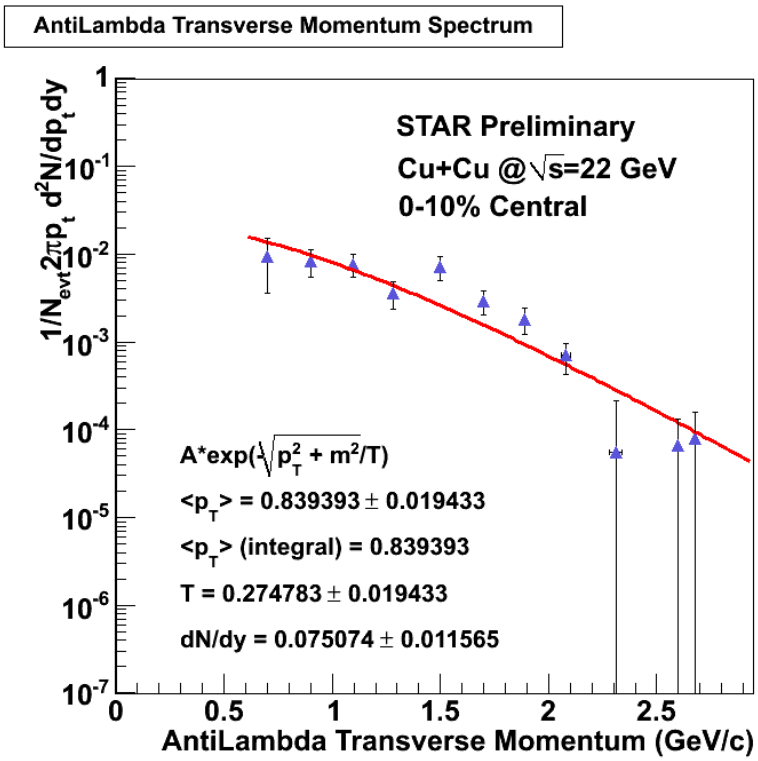

Figure 38: Anti-Lambda Transverse Momentum Spectrum, 0-10% Centrality

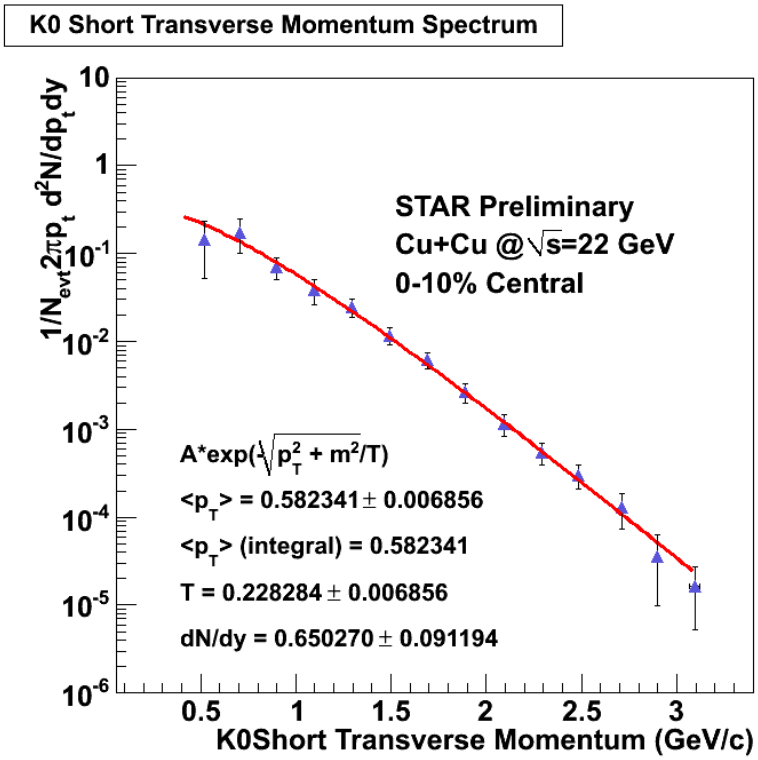

Figure 39: K0-Short Transverse Momentum Spectrum, 0-10% Centrality

4.4 Embedding Comparison

As a quality assurance check on the embedding and efficiency corrections, the embedded particles should be compared to the particles in the actual data to ensure that the embedding accurately reflects the physical data being collected. Figures 40, 41, and 42 show the DCA of daughters, decay length, DCA to primary vertex, NHits for positive/negative daughters, and DCA of positive/negative daughters to the primary vertex.

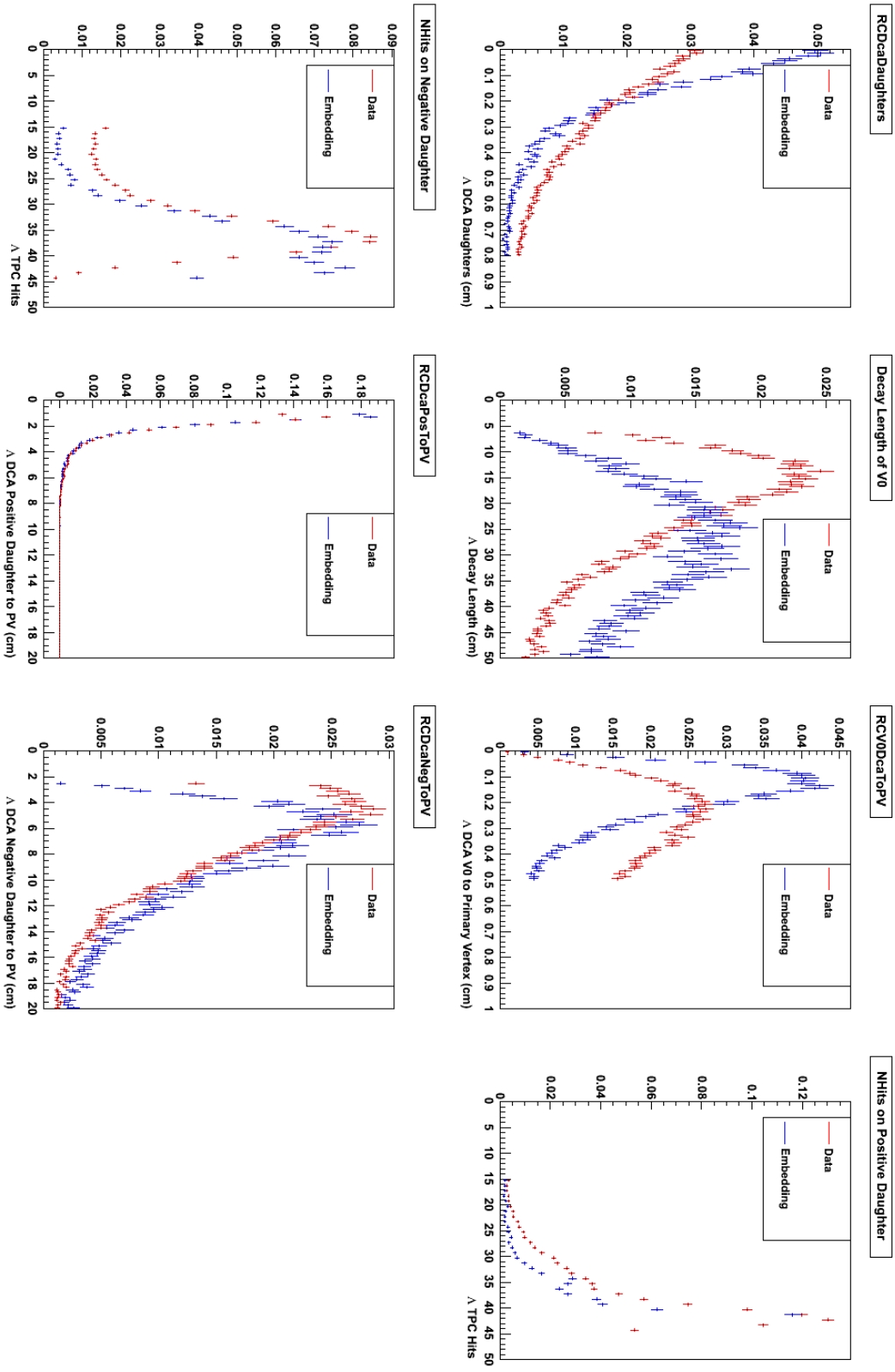

Figure 40: Embedding Comparison for Lambdas

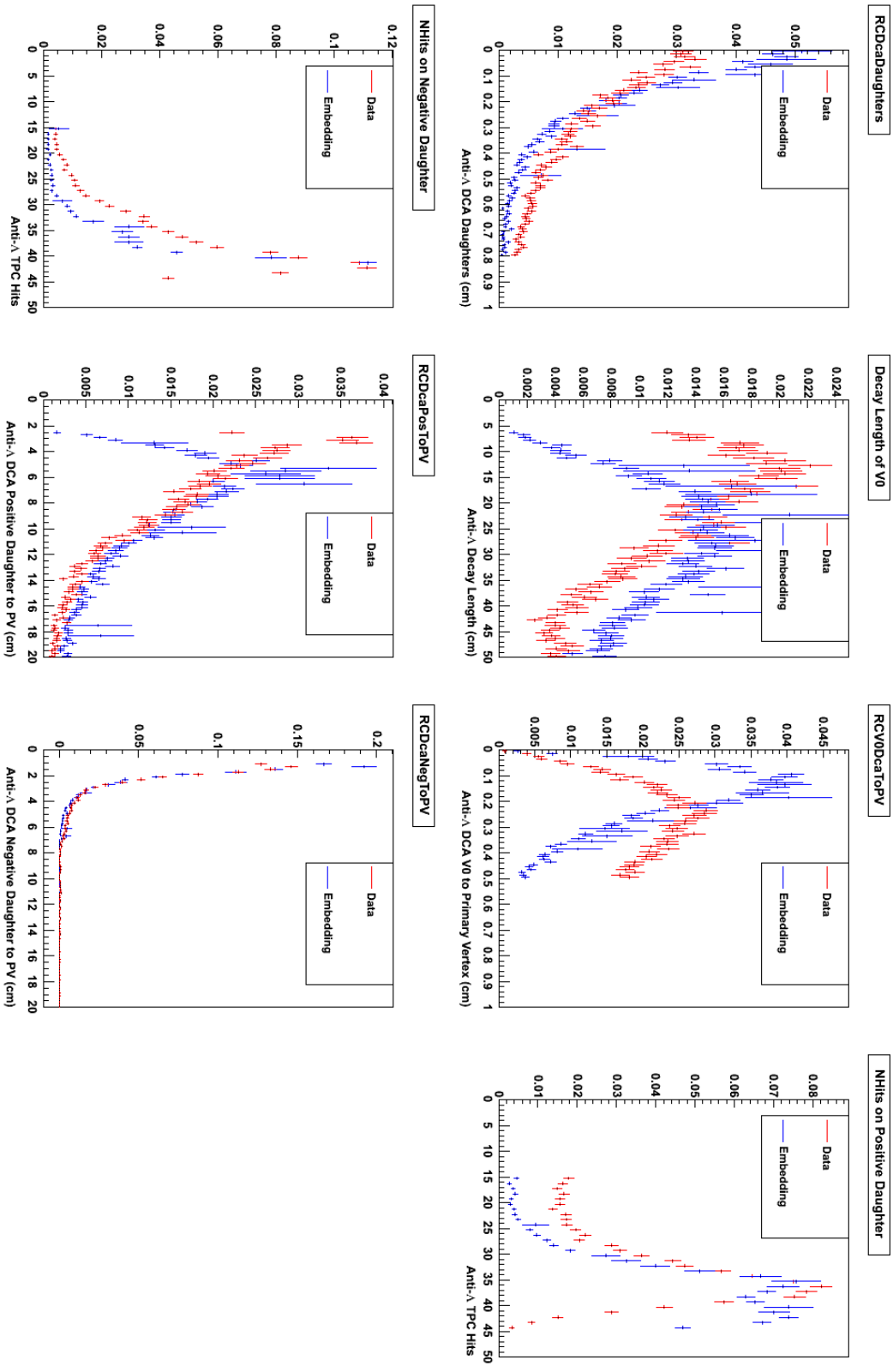

Figure 41: Embedding Comparison for Anti-Lambdas

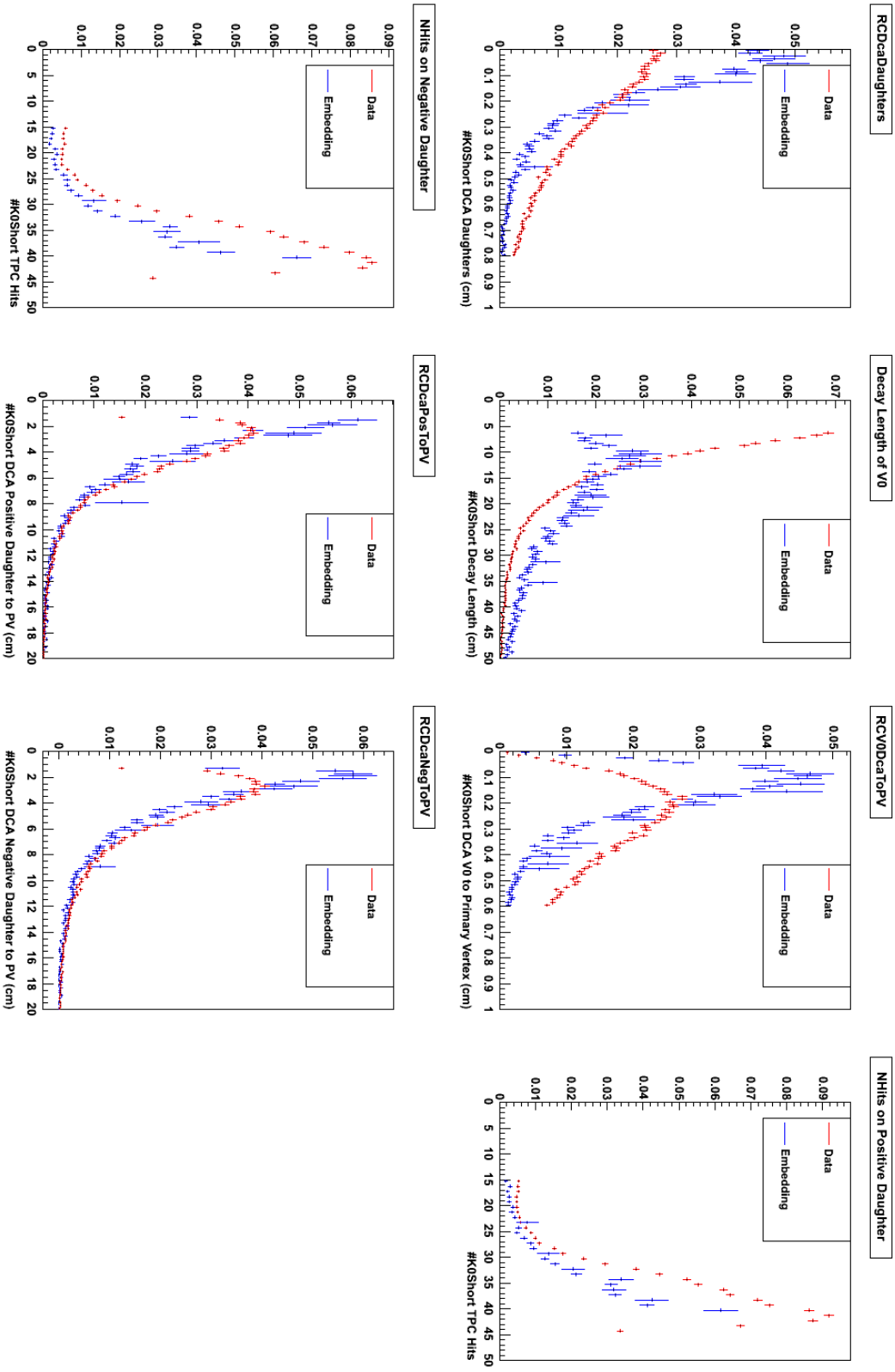

Figure 42: Embedding Comparison for K0-Shorts

Most of the embedding data seems to follow the same trends as the actual physical data from STAR, which provides confidence in the embedding. A discrepancy is noticed, however, in the plots for V0 decay length and DCA of V0 to the primary vertex. Figures 43 and 44 show these plots again for the example of a Λ, but broken down into different transverse momentum bins this time. Within their corresponding bins of p_t, these distributions for V0 decay length and DCA of V0 to the primary vertex agree. What appeared as a discrepancy was due to the fact that the average V0 decay length and DCA of V0 was different across all momenta, but these figures show that the embedded particles and actual data actually do agree within each bin of momentum. This is because the embedding statistics are much larger than the actual data in the high p_t bins, so the embedding distribution has a different shape. Since the corrections are applied bin by bin, the corrections, hence, remain validated.

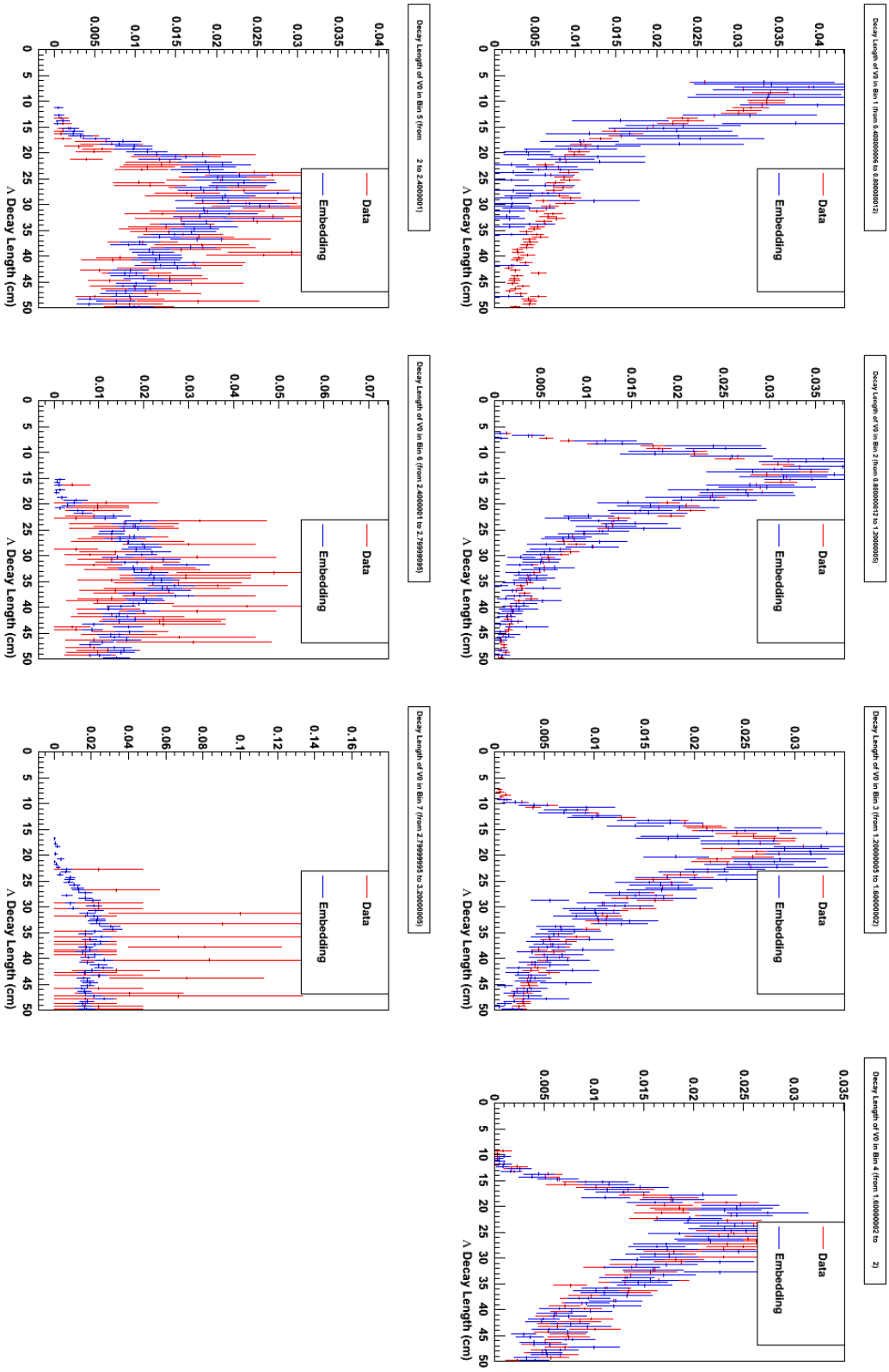

Figure 43: Lambda Decay Length Embedding Comparison

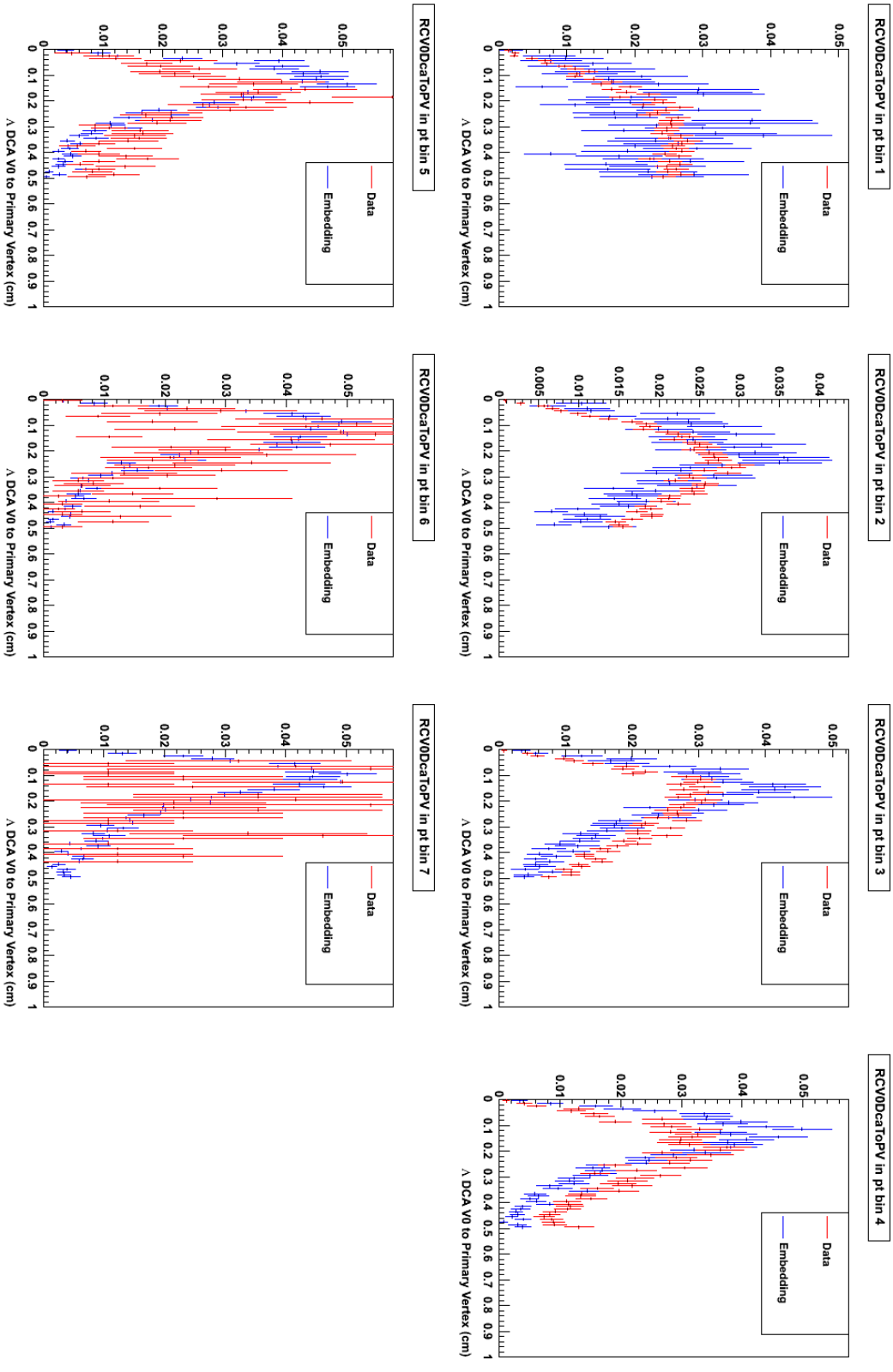

Figure 44: DCA Lambda to Primary Vertex Embedding Comparison

Chapter 5 – Discussion

The total yield of Λ's, Anti-Λ's, and K_S^0's for each centrality range for this particular collision system can be used in multiple analyses. Most notable in this project is the determination of the dependence of strangeness production on the system size and collision energy. The data in this experiment can be contrasted with itself and data from other experiments to explore these topics. In this chapter, the strangeness yield and Anti-Λ to Λ ratio are examined in light as functions of energy and system size. Also, the Λ to K_S^0 ratio is displayed to explore the formation of baryons versus mesons in windows of transverse momentum.

5.1 Anti-Lambda to Lambda Ratio

The ratio of Anti-Λ to Λ particles was calculated for each bin of momentum in each centrality. Every quark in an Anti-Λ is produced in the collision. Λ's are more prevalent since they are matter, and the STAR detector may find some that contain quarks from the baryons involved in the collision. As the yield of Anti-Λ's in a collision approaches the yield of Λ's, the collision is more "baryon-free." The measurement of how baryon-free a collision is indicates how much influence remained from the baryons in the incoming nuclei as opposed to the energy of the collision. As the ratio of Anti-Λ's to Λ's approaches 1, the matter that is being detected comes increasingly from the energy of the collision rather than from the baryons that carried the

energy into the collision area. Figures 45, 46, and 47 show the Anti-Λ to Λ ratios for the three centralities. Because this is a ratio, the correction factors divide out of this plot. The ratio shows no p_t dependence over the observed range. The line is a fit of a constant, assuming that the ratio is flat over p_t.

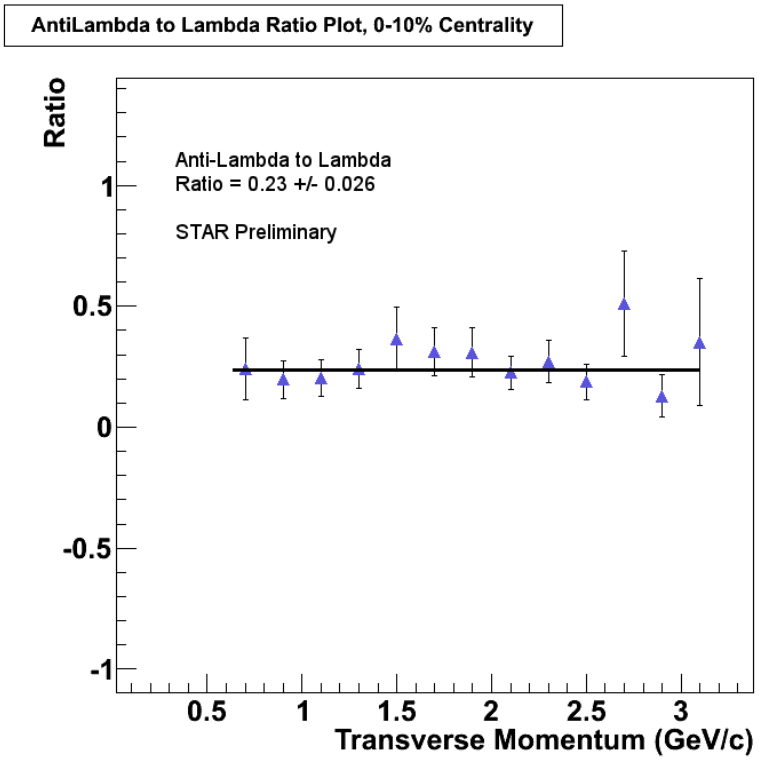

Figure 45: Anti-Lambda to Lambda Ratio, 0-10% Centrality

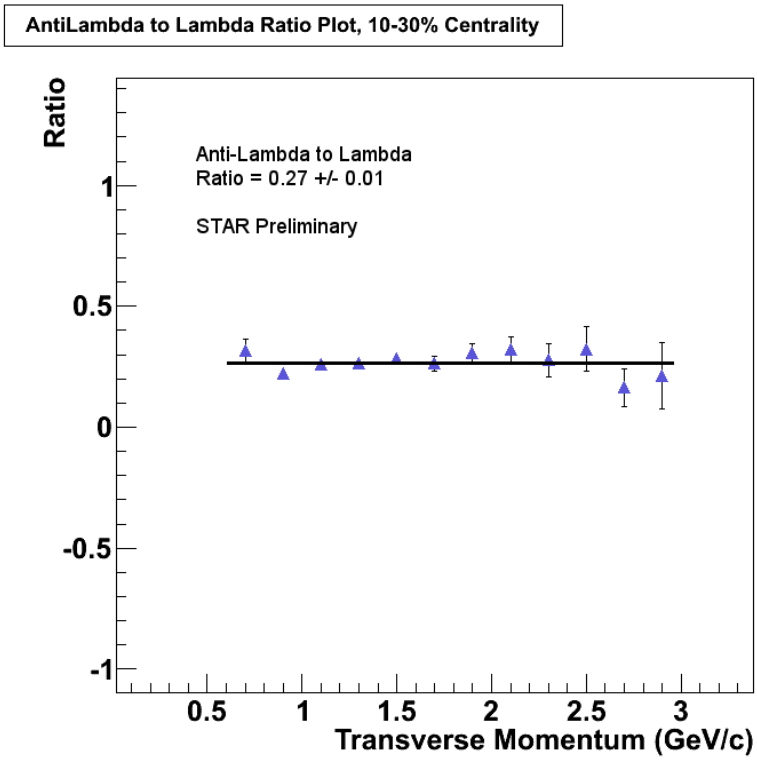

Figure 46: Anti-Lambda to Lambda Ratio, 10-30% Centrality

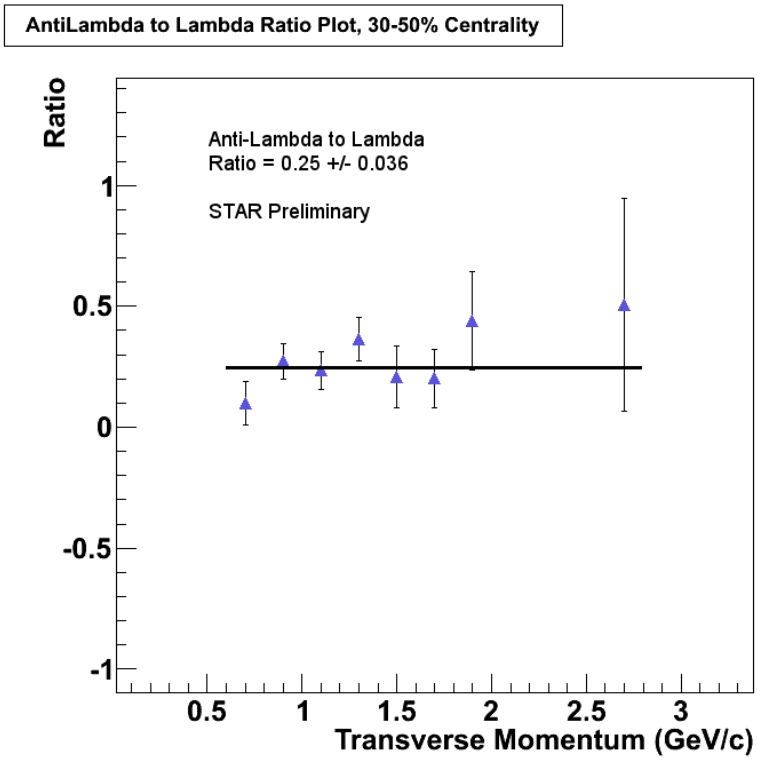

Figure 47: Anti-Lambda to Lambda Ratio, 30-50% Centrality

5.2 Energy Dependence

The strangeness yield of copper-copper collisions can be compared at different energies in order to determine how the energy of a collision affects strange particle production. Additionally, the Anti-Λ to Λ ratio can be compared to ratios calculated from other analyses at different energies, regardless of the size of the ions involved.

5.2.1 Energy Dependence of Yield

The yield of Λ's and K_S^0's at the highest centrality for this experiment was compared to the yields for other copper collisions at STAR at 62 GeV per nucleon and 200 GeV per nucleon.

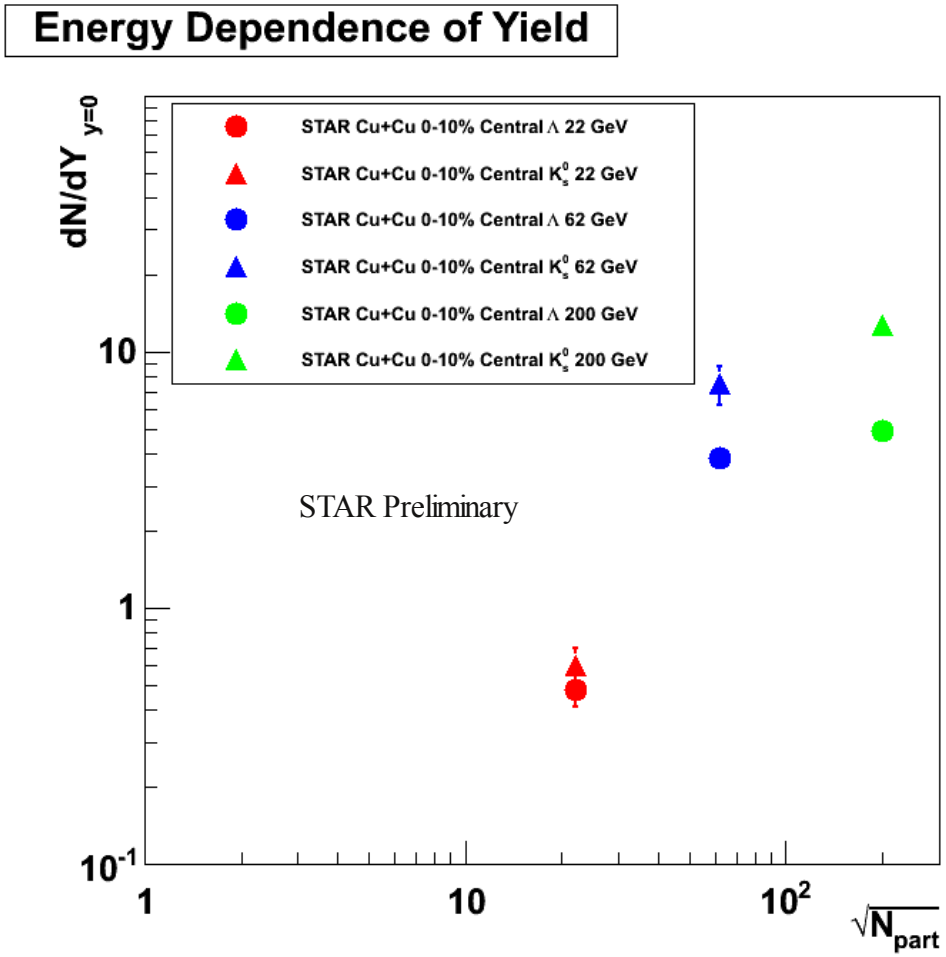

Figure 48: Energy Dependence of Yield for Lambda and K0-Shorts, Cu+Cu Collisions

As evidenced in Figure 48, the strangeness production increases with increasing collision energy. The production of K_S^0's increases relative to the production of Λ's as energy increases. The production of both species appears to be approaching saturation at a collision energy of about 200 GeV.

5.2.2 Energy Dependence of Anti-Lambda to Lambda Ratio

The ratio of Anti-Λ's to Λ's at the 0-10% centrality for this analysis was compared to the rest of the world's data, with varying energies and sizes of nuclei. As shown in Figure 49, the ratio falls in line with the other data where it would be expected for this energy. This ratio shows that the degree to which a collision is baryon-free is dependent on energy and independent from system size, so a Cu nucleus is not more transparent than an Au nucleus. A net baryon-free collision area is desirable because it indicates that the baryons detected are more heavily influenced by energy, not the baryons involved in the collision. As shown in Figure 49, the highest energy collisions have an Anti-Λ to Λ ratio closest to 1 and are the most baryon-free. An Anti-Λ to Λ ratio close to 1 is expected for baryon-free collisions because the baryon number is zero for baryon-free collisions. As described previously, a baryon number of zero will result in the same amount of baryons as anti-baryons detected. In lower energy collisions, many of the baryons being detected are not from the energy of the collision or the quark-gluon plasma freeze-out, but are fragments from the collision matter.

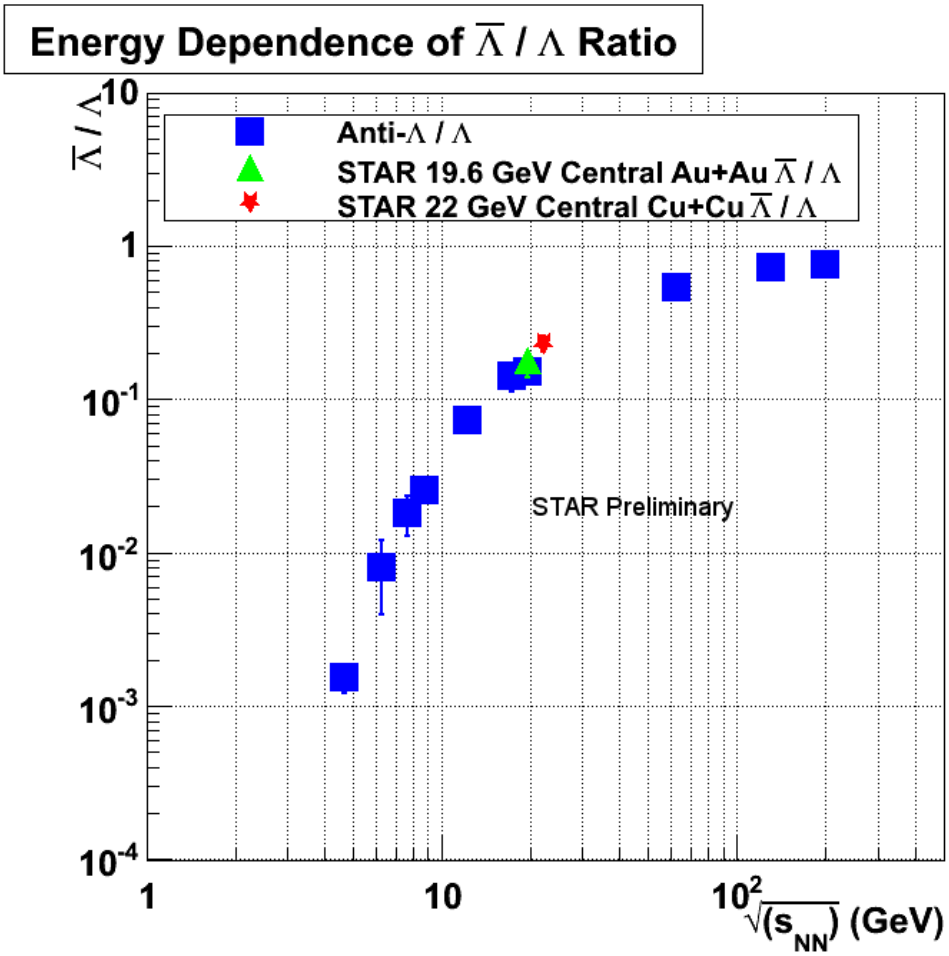

Figure 49: Energy Dependence of Anti-Lambda to Lambda Ratio

5.3 System Size Dependence

In the same way that strangeness yield and the Anti-*Λ* to *Λ* ratio can be plotted against energy, they can also be plotted against the number of participants in a collision, indicating the system size. $\langle N_{part} \rangle$ is the average number of nucleons involved in a collision event. It is dependent on centrality of the collision and the size of the nuclei. $\langle N_{part} \rangle$ was calculated for each centrality using a Glauber model calculation [10], which uses the centrality of events and the size of the ions involved to determine the average number of nucleons involved in a given event [3].

5.3.1 System Size Dependence of Yield

The yield of Λ's and Anti-Λ's for this experiment was plotted as a function of $<N_{part}>$ in Figure 50. The blue point with the lowest $<N_{part}>$ is hidden underneath the red point with the lowest $<N_{part}>$. In this experiment, the yield of strange particles increased along with the average number of nucleons involved in the collision. This trend is nearly linear on the plot when dN/dY is plotted on a logarithmic scale. In the most central collisions, there are signs of saturation occurring.

Figure 51 shows the yield of Λ's and Anti-Λ's as a function of $<N_{part}>$ plotted for copper ion collisions at 22 GeV and gold ion collisions at 19.6 GeV. Ideally, one would expect the two

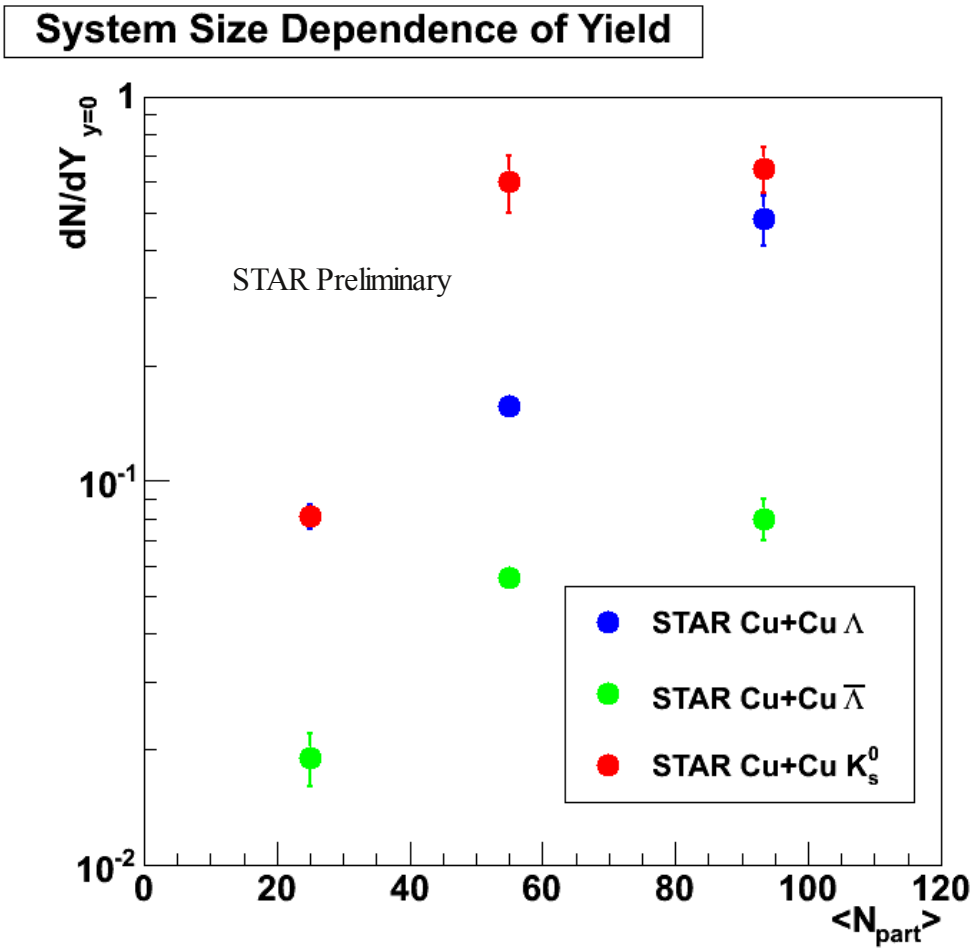

Figure 50: System Size Dependence of Lambda, Anti-Lambda, and K0-Short Yield

curves for the different collision systems to meet where their calculated <N_{part}> is the same. Instead, there is a vertical shift that is exhibited between the data analyzed by Kyle Englund-Krieger in Au+Au collisions in 2010 and the data analyzed in this Cu+Cu experiment [9]. The results for this analysis appear to be under-corrected. The current belief is that the under-correction is due to the trigger mix used in the data collection and the apparently wide variation in trigger efficiency. This variation will require a further correction to account for trigger

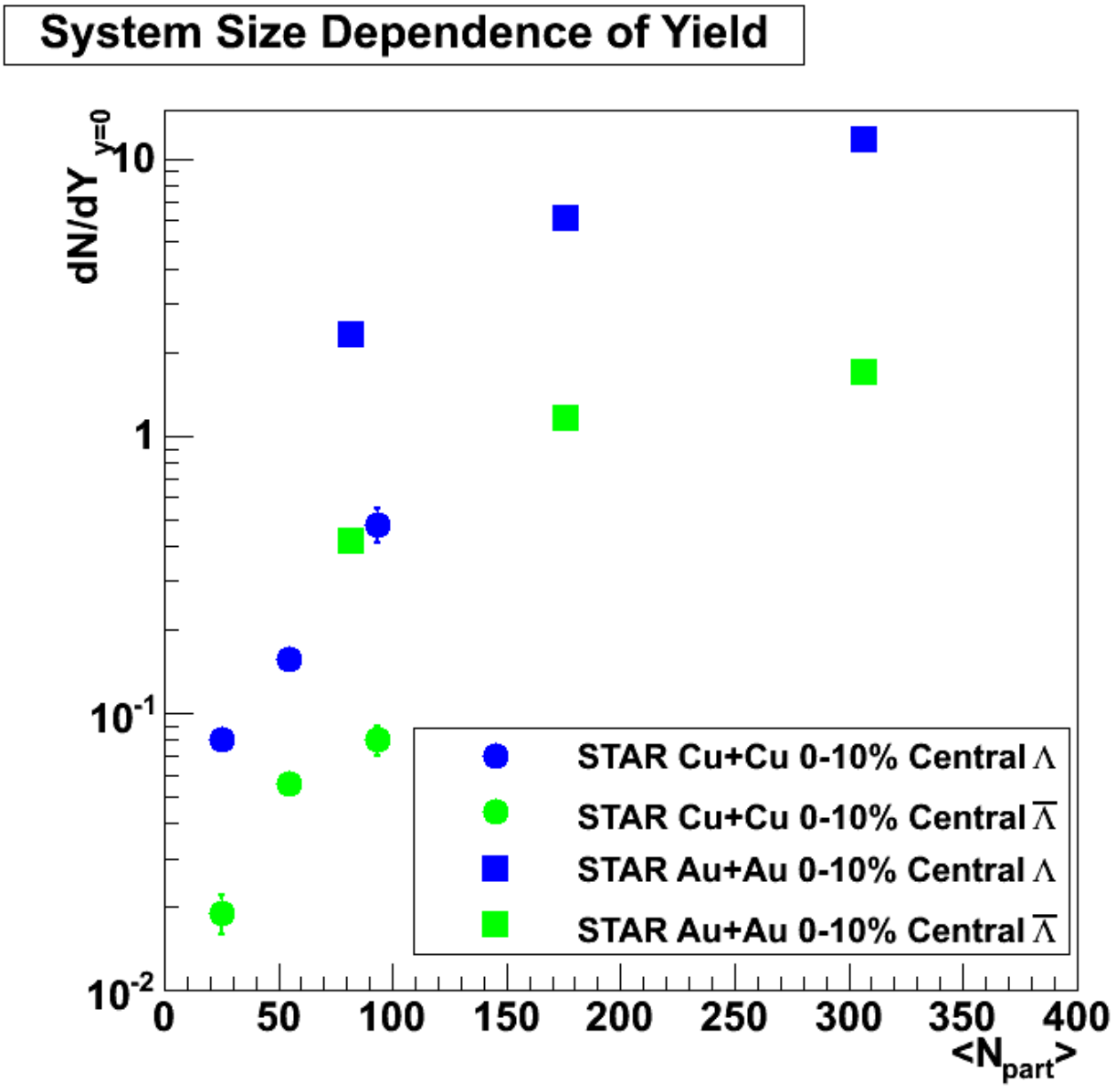

Figure 51: System Size Dependence of Lambda and Anti-Lambda Yield, Cu+Cu and Au+Au Collisions

efficiency. However, Figure 51 demonstrates qualitatively, if not strictly quantitatively, the trend that yield increases with increasing <N_{part}>.

5.3.2 System Size Dependence of Anti-Lambda to Lambda Ratio

The Anti-Λ to Λ ratios for each centrality in this calculation and an Au+Au analysis at 19.6 GeV per nucleon were plotted against <N_{part}> in Figure 52. This plot shows that the collisions with fewer participating nucleons are generally more baryon-free. This trend is similar for both the copper and gold collisions separately, although the gold collisions access a greater region of <N_{part}>. For each, the least and mid-central points have an Anti-Λ to Λ ratio that is

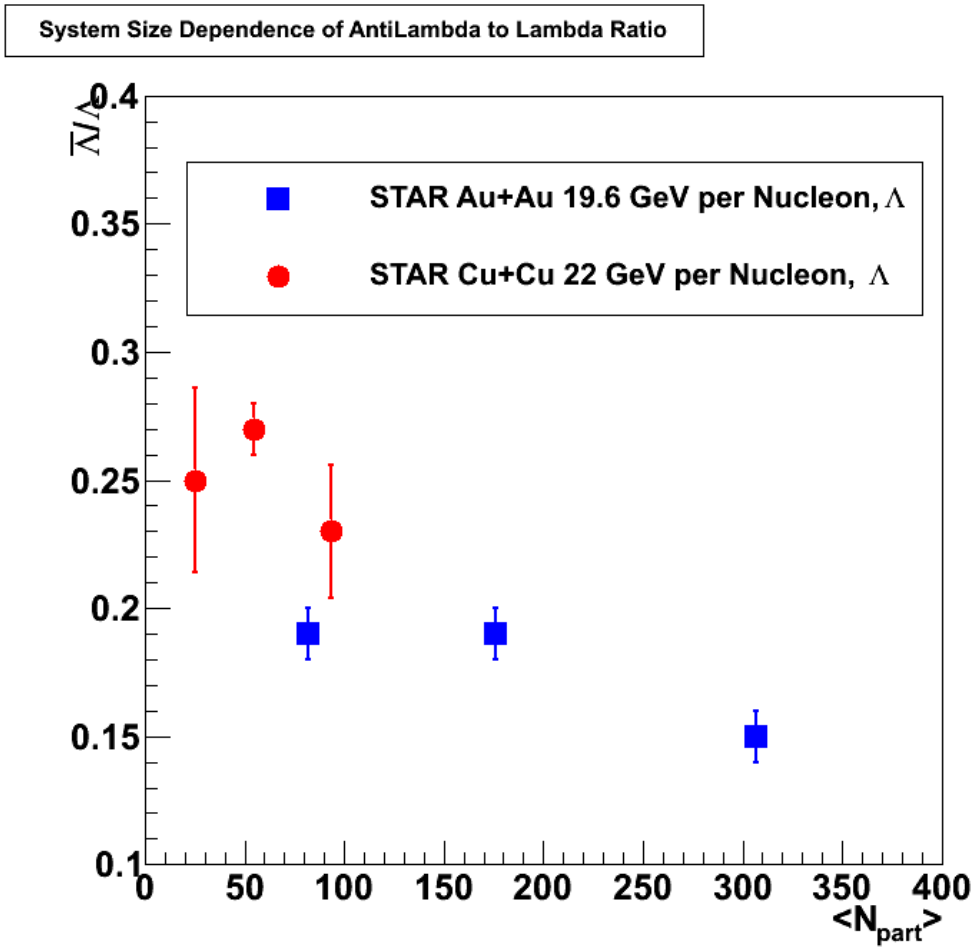

Figure 52: System Size Dependence of Anti-Lambda to Lambda Ratio

approximately the same while the most central point drops slightly. The two datasets roughly meet within error bars. Unlike the discrepancies described in Figure 51, the correction factor affects the Anti-Λ and the Λ in the same way in the Anti-Λ to Λ ratio, so the shift observed previously, possibly due to trigger inefficiencies, is not present in this observable.

5.4 Lambda to K0-Short Ratio

The Λ to K_S^0 ratio is plotted in Figure 53 for each bin of momentum for 0-10% and 10-30% centralities. For both centralities, more K_S^0's (mesons) are produced relative to Λ's (baryons) at low and high regions of transverse momentum. At mid-regions of transverse

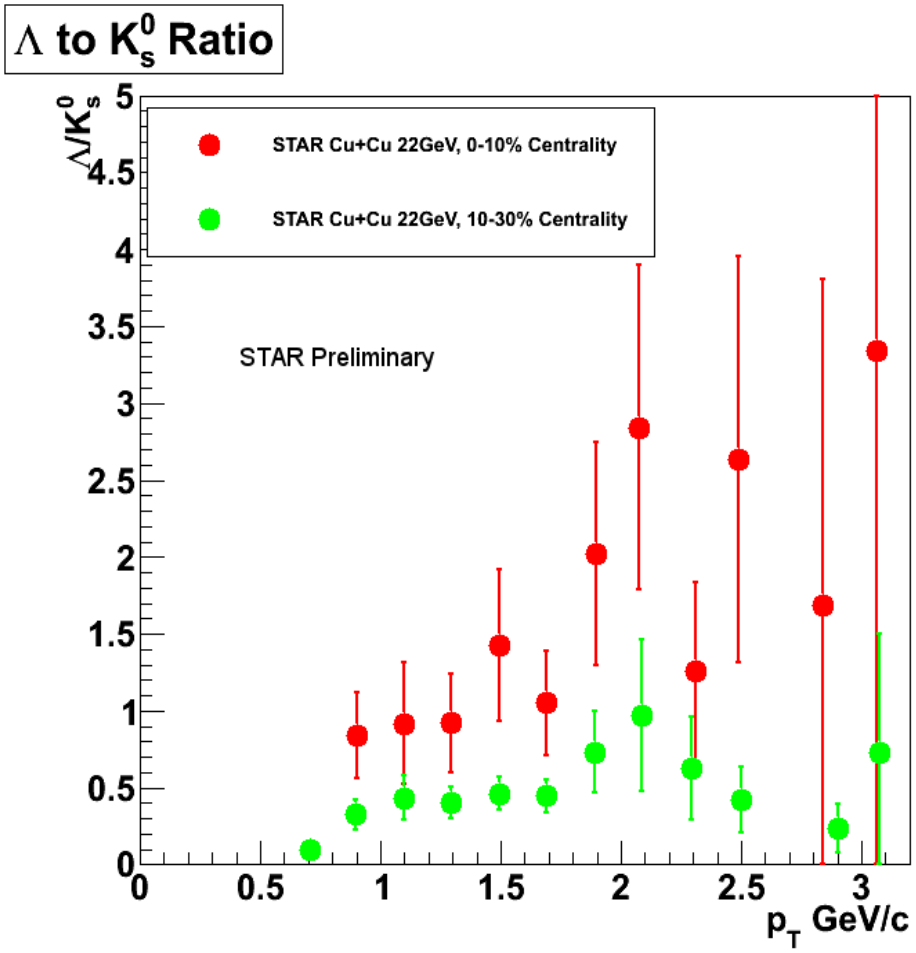

Figure 53: Lambda to K0-Short Ratio Vs. Transverse Momentum

momentum, more baryons are expected to form due to quark coalescence, the process by which co-moving quarks recombine as quark-gluon plasma freezes out [11]. If quarks are moving away from the collision area in a certain window of momentum and nearby in space, they are more likely to meet and join with the other quarks needed to produce a baryon such as a Λ [12]. At high regions of transverse momentum, the production of mesons dominate as they are produced through jets of fragmenting quarks and anti-quarks [11],[12]. Quark or anti-quark fragmentation at high-p_t is more likely to form mesons as new quarks and anti-quarks are thought to be produced pairwise rather than in triplets [12]. Although the error bars on the graph are quite large, the window of momentum for relatively greater baryon production can be qualitatively seen with its peak at about the 2.1 GeV/c mark of transverse momentum. Greater statistics are needed to reduce the error bars and extend the measured p_t range.

Chapter 6 – Conclusion

The search for the critical point of hadronic matter will continue as more systematics are added to the dataset on the behavior of nuclear matter in extreme conditions. The yields and ratios calculated in this analysis add to those systematics and have applications beyond even those addressed in this paper. The data from this analysis will be accessible to other researchers in the heavy-ion community for comparison and study and to theorists for refining current models. Trends in system size and energy dependence were examined in both qualitative and quantitative ways, showing how strangeness production and the Anti-Λ to Λ ratio depend on the number of participating nucleons and the center-of-mass energy of the particles in the collision. Further study of the variation of trigger efficiency will be needed to allow comparison with other data in observables affected by the trigger mix. Also, the development and use of the STAR embedding chain at USNA has recovered capabilities for the experiment that have not existed since 2009.

This project examined strangeness production's dependence on collision energy and system size. It concluded that collisions with higher center-of-mass energies are more baryon-free. Strangeness yield was found to increase with an increase in energy per nucleon, with the production of some particles appearing to saturate at higher energies for the production of some particles. Collisions with more participants were observed to be less baryon-free than than those with less participants. Strangeness yield increased when the system size and centrality increased,

saturating at higher numbers of participating nucleons. The project supplied additional systematics that contribute to the knowledge of nuclear matter's behavior in extreme conditions. These conclusions contribute to the ongoing investigation for the critical point and of the behavior of QGP.

References

[1] M. Riordan W. Zajc, "The First Few Microseconds," Sci. Am. **294**, 34-41(2006) [doi:10.1038/scientificamerican0506-34A].

[2] M. Lamont, "Neutral Strange Particle Production in Ultra-Relativistic Heavy Ion Collisions at $\sqrt{s_{NN}}$ = 130 GeV," Thesis Submitted to the University of Birmingham (2002).

[3] A. Timmins, "Neutral Strange Particle Production in Relativistic Cu+Cu Collisions at $\sqrt{s_{NN}}$ = 200 GeV," Thesis Submitted to the University of Birmingham (2008).

[4] J. Mitchell, "RHIC and the Pursuit of the Quark-Gluon Plasma," Prepared for Brookhaven National Laboratory (2001) [BNL-68850].

[5] "The STAR Time Projection Chamber: A unique tool for studying high multiplicity events at RHIC," Nucl. Instrum. Meth. **A 499**, 659 (2003).

[6] "Solenoidal Tracker at RHIC: Conceptual Design Report," STAR Collaboration, Web Only, (1992). Available online to read at http://drupal.star.bnl.gov/STAR/files/StarCDR.pdf

[7] "RHIC Accelerators," Brookhaven National Laboratory, Web Only. Available online at http://bnl.gov/rhic/RHIC_complex.htm

[8] K. Ackermann *et al.*, Nucl. Phys. **A 661**, 681c (2001)

[9] K. Englund-Krieger, “Strangeness Production in 19.6 GeV Collisions at the Relativistic Heavy Ion Collider,” Trident Scholar Report, United States Naval Academy (2010) [No. 387]

[10] Bialas, Bleszynski, and Czyz, Nucl. Phys. **B 111**, 461(1976)

[11] A. Timmins, “Strangeness Production in Heavy-Ion Collisions at STAR,” Nucl. Phys. **A 830**, 829c-832c (2009)

[12] R.C. Hwa and X.N. Wang, World Scientific, Singapore, (2003) [nucl-th/0305084]